Developmental Cell

Volume 24
Number 2

January 28, 2013

www.cellpress.com

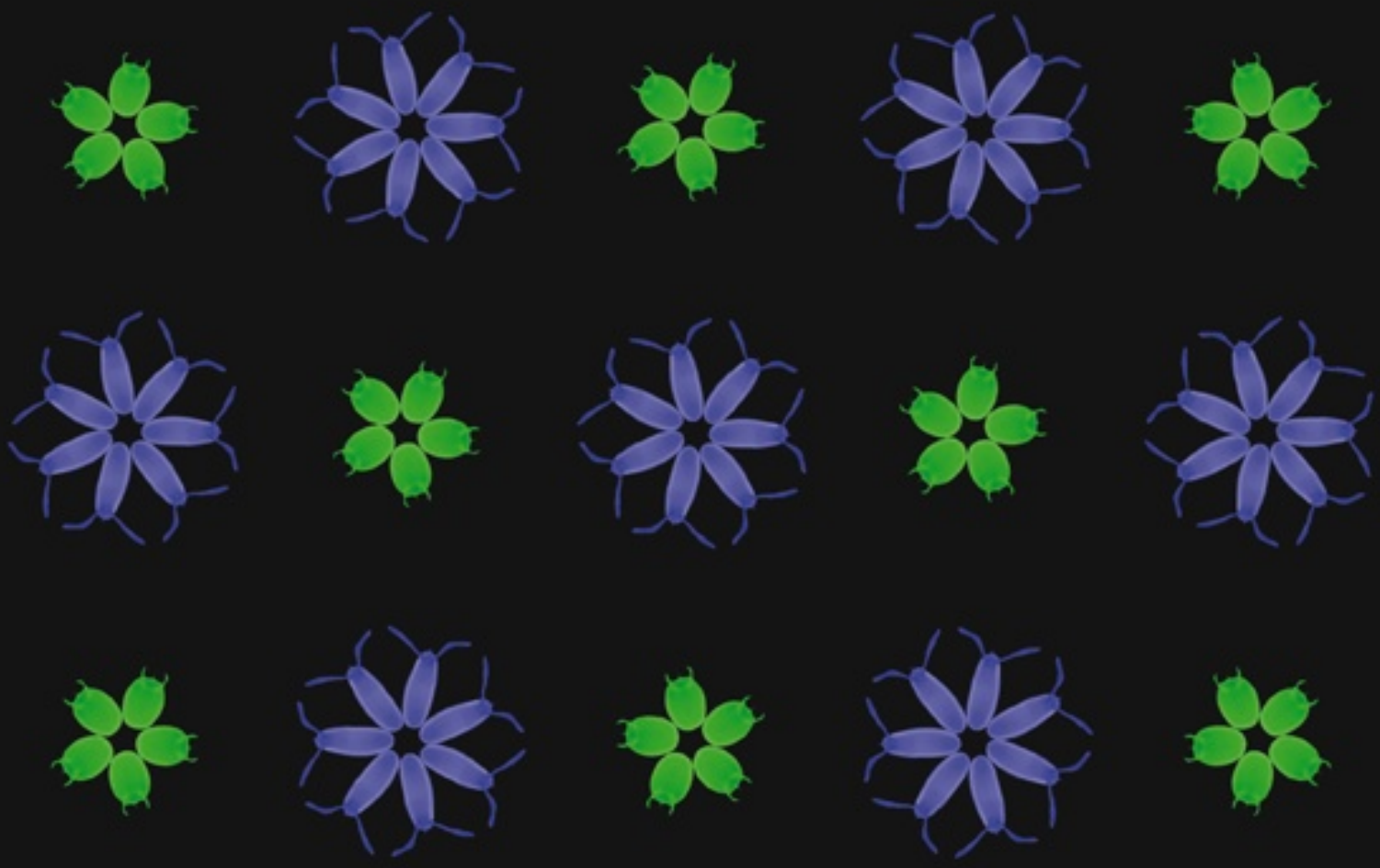

Polarized Basement Membrane Secretion

Developmental Cell
Article

A Rab10-Dependent Mechanism for Polarized Basement Membrane Secretion during Organ Morphogenesis

David W. Lerner,[1] Darcy McCoy,[1,3] Adam J. Isabella,[2,3] Anthony P. Mahowald,[1,2] Gary F. Gerlach,[1,4] Thymur A. Chaudhry,[1,5] and Sally Horne-Badovinac[1,2,*]
[1]Department of Molecular Genetics and Cell Biology
[2]Committee on Development, Regeneration and Stem Cell Biology
The University of Chicago, Chicago, IL 60637, USA
[3]These authors contributed equally to this work
[4]Present address: Biological Sciences Graduate Program, University of Notre Dame, Notre Dame, IN 46556, USA
[5]Present address: Medical College, Rush University, Chicago, IL 60612, USA
*Correspondence: shorne@uchicago.edu
http://dx.doi.org/10.1016/j.devcel.2012.12.005

SUMMARY

Basement membranes (BMs) are specialized extracellular matrices that are essential for epithelial structure and morphogenesis. However, little is known about how BM proteins are delivered to the basal cell surface or how this process is regulated during development. Here, we identify a mechanism for polarized BM secretion in the *Drosophila* follicle cells. BM proteins are synthesized in a basal endoplasmic reticulum (ER) compartment from localized mRNAs and are then exported through Tango1-positive ER exit sites to basal Golgi clusters. Next, Crag targets Rab10 to structures in the basal cytoplasm, where it restricts protein delivery to the basal surface. These events occur during egg chamber elongation, a morphogenetic process that depends on follicle cell planar polarity and BM remodeling. Significantly, Tango1 and Rab10 are also planar polarized at the basal epithelial surface. We propose that the spatial control of BM production along two tissue axes promotes exocytic efficiency, BM remodeling, and organ morphogenesis.

INTRODUCTION

Basement membranes (BMs) are an ancient form of extracellular matrix found at the basal surface of all epithelia (Yurchenco, 2011). Although often overlooked as passive scaffolds, these complex protein lattices provide many essential functions to neighboring cells. In addition to providing tissue support, BMs act as signaling platforms for cell polarization, stem cell regulation, and migrating organ primordia (Arnaoutova et al., 2012; Bunt et al., 2010; Mirouse et al., 2009; O'Brien et al., 2001; Schneider et al., 2006; Wang et al., 2008). They also play central roles in organ morphogenesis and physiology (Fata et al., 2004; Miner, 2011; Miner and Yurchenco, 2004; Pastor-Pareja and Xu, 2011; Urbano et al., 2009). The misregulation of BM structure can be a hallmark of tumor progression (Valastyan and Weinberg, 2011). Despite these critical functions, we know relatively little about the molecular control of BM assembly.

BMs are primarily composed of type IV collagen (Col IV), laminin, nidogen, and heparan sulfate proteoglycans such as perlecan or agrin. Among these components, Col IV predominates, representing up to 50% of BM proteins (Kalluri, 2003). Despite its abundance, the pathway for Col IV production is complex. Each Col IV molecule is composed of three polypeptides, two α1 chains and one α2 chain, that initiate contact at their C termini and then assemble into a triple helix, ~400 nm long (Khoshnoodi et al., 2008). Col IV folding requires a suite of endoplasmic reticulum (ER)-resident enzymes and chaperones, many of which are Collagen-specific (Myllyharju and Kivirikko, 2004). These proteins include lysyl- and prolyl-hydroxylase enzymes that modify the α chains both during and after translation. Special mechanisms also facilitate Col IV export. Newly synthesized proteins typically leave the ER in COPII-coated vesicles that are too small to accommodate the extended Col IV trimer (Fromme and Schekman, 2005; Jin et al., 2012; Malhotra and Erlmann, 2011). The transmembrane cargo receptor Tango1 is required at transitional ER (tER) sites to help package collagens into enlarged Golgi-bound vesicles (Saito et al., 2009; Venditti et al., 2012; Wilson et al., 2011).

Following their synthesis, new BM proteins must be targeted to the proper membrane domain for secretion. Polarized epithelial cells have distinct apical, junctional, lateral, and basal membrane domains, each of which contains a unique complement of lipids and proteins. These domains are established and maintained by polarized vesicle traffic that delivers newly synthesized secreted and transmembrane proteins to the appropriate cell surface (Mellman and Nelson, 2008; Rodriguez-Boulan et al., 2005). Although much is known about the trafficking pathways that target transmembrane proteins to the combined basal and lateral surfaces, there have long been indications that BM proteins reach the basal surface through a distinct mechanism (Boll et al., 1991; Caplan et al., 1987; Cohen et al., 2001; De Almeida and Stow, 1991). The first molecular evidence for this assertion came from genetic studies in *Drosophila* that identified the DENN domain protein, Crag, and the protease-like protein, Scarface (Scaf), as selective regulators

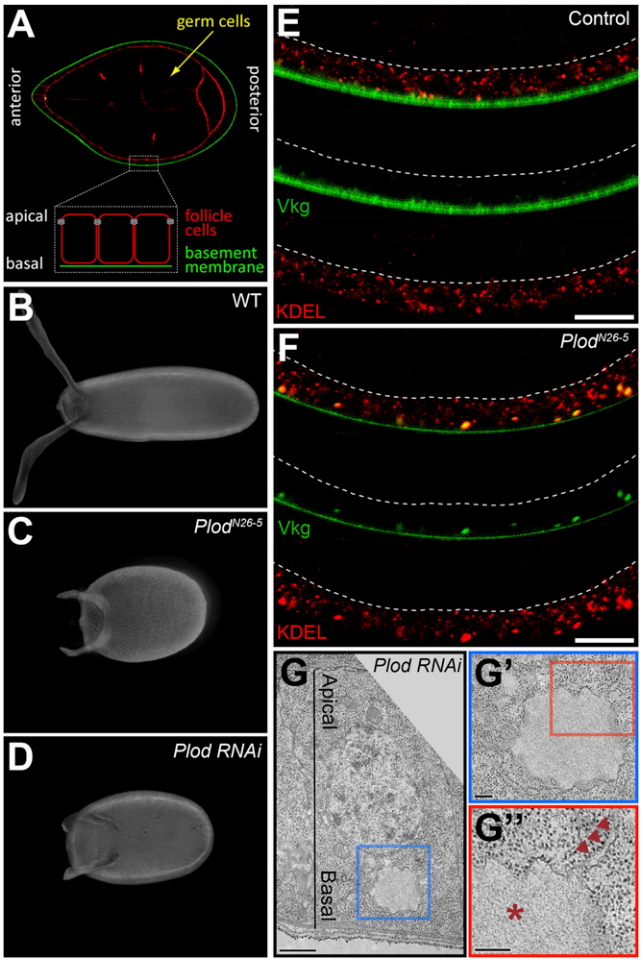

Figure 1. *Plod*$^{N26-5}$ Disrupts the Secretion of Col IV

(A) Overview of egg chamber structure at stage 8. Actin (red), Vkg-GFP (green). (B–D) Representative egg shapes for wild-type (B), *Plod*$^{N26-5}$ (C), and *Plod-RNAi* (D).

(E) In wild-type, proteins with the KDEL ER retention signal are throughout the cell, whereas Vkg-GFP is in the BM. Dashed lines mark the apical surface. Scale bar represents 10 μm. Experiments performed at stages 7–8.

(F) In *Plod*$^{N26-5}$, Vkg-GFP punctae overlap with KDEL near the basal surface, indicating ER accumulation. Dashed lines mark the apical surface. Scale bar represents 10 μm. Experiments performed at stages 7–8.

(G) TEM of a single *Plod-RNAi* follicle cell showing a distended ER region in the basal cytoplasm. Scale bar represents 1 μm. Experiments performed at stages 7–8.

(G′ and G″) Magnifications of the image in (G). Ribosomes decorate the distended ER cisterna (asterisk) and adjacent, normal ER membranes (arrowheads). Scale bars represent 200 nm.

See also Figure S1.

of polarized BM deposition (Denef et al., 2008; Eastburn and Mostov, 2010; Sorrosal et al., 2010). Loss of either gene causes BM proteins to accumulate on both the basal and apical epithelial surfaces without obvious effects on other exocytic cargo. Currently, the mechanisms by which Crag and Scaf promote polarized BM secretion are unknown.

The *Drosophila* egg chamber provides a highly tractable system for the study of BM biology in the context of a developing organ. Egg chambers are multicellular structures within fly ovaries that will each give rise to a single egg. They are composed of an inner germ cell cluster surrounded by an outer epithelial layer of follicle cells. The apical follicle cell surfaces face the germ cells, whereas the basal surfaces contact the BM (Figure 1A). The BM, in turn, forms the egg chamber's outer most layer. To our knowledge, the follicle cells are the only fly epithelium that synthesizes all major BM components (Mirre et al., 1988; Pastor-Pareja and Xu, 2011; Yasothornsrikul et al., 1997).

Interestingly, the follicle cell BM plays a critical role in shaping the fly egg. Though initially spherical, egg chambers lengthen along their anterior-posterior (AP) axes as they develop. This morphogenesis depends on an unusual form of planar polarity, in which actin filaments at the basal cell surface become aligned orthogonal to the AP axis (Gutzeit, 1990). Once oriented, the follicle cells undergo a directed migration along the inner BM surface, a process that causes the entire egg chamber to rotate inside the stationary matrix (Haigo and Bilder, 2011). Importantly, the migrating follicle cells also secrete new BM proteins. Through a process that is still poorly understood, the combination of cell movement and matrix secretion creates fibril-like structures in the BM, perpendicular to the elongation axis (Gutzeit et al., 1991; Haigo and Bilder, 2011; Schneider et al., 2006) (Figure S1A available online). It has been proposed that this fibrillar matrix then constrains isometric egg chamber growth to promote AP elongation, but many questions remain about how this unusual BM structure is built.

Here, we identify a mechanism for polarized BM secretion in the follicle cells. Starting from a mutation that traps Col IV in the cell, we show that BM proteins are locally synthesized in a basal ER compartment, and are exported through Tango1-positive ER exit sites to basal Golgi clusters. We then introduce Rab10 as a regulator of polarized BM secretion, and show that Crag regulates Rab10 in this context. Finally, we show that the BM exocytic machinery is also planar polarized at the basal epithelial surface. Our data suggest that BM proteins are secreted from the trailing edge of each migrating follicle cell, a process that may contribute to the formation of BM fibrils and egg chamber elongation. We therefore propose that the spatial regulation of BM production along two tissues axes promotes both polarized secretion and matrix remodeling during organ morphogenesis.

RESULTS

Col IV Accumulates in a Basal ER Region in *Plod* Mutant Follicle Cells

We have previously reported a genetic screen for mutations that block egg chamber elongation and produce round eggs (Horne-Badovinac et al., 2012). The RE-H complementation group from this screen contained a single allele, *N26-5* (Figures 1B and 1C). We used deficiency mapping to localize *N26-5* to a chromosomal region containing the *procollagen lysyl hydroxylase* (*Plod*) gene. Sequencing the *Plod* coding regions in *N26*-5 mutant larvae identified a lesion, which is predicted to change a highly conserved glycine to aspartic acid in one of the protein's catalytic domains (Figure S1B). RNAi knockdown of Plod in the

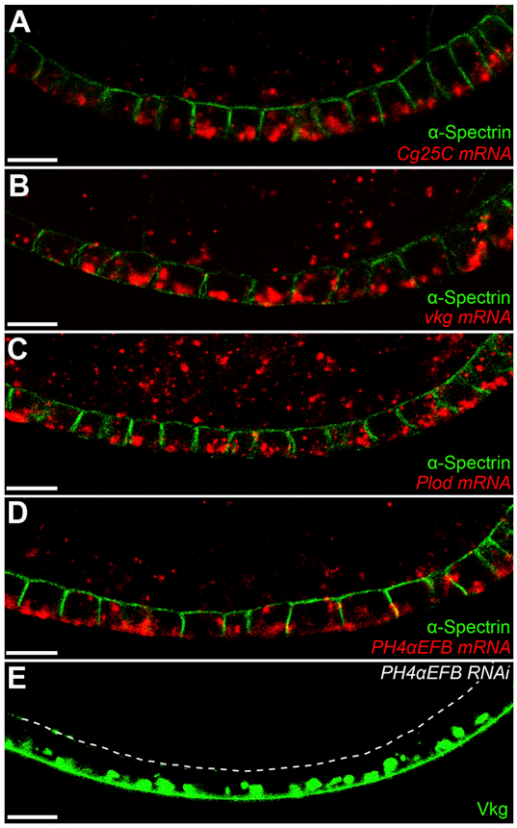

Figure 2. Col IV Is Synthesized in the Basal ER

(A–D) mRNAs encoding the Col IV α chains Cg25C (A) and Vkg (B), and the Col IV biosynthetic enzymes Plod (C) and PH4αEFB (D) are all enriched in the basal cytoplasm. α-Spectrin marks the apical and lateral epithelial surfaces.

(E) *PH4αEFB-RNAi* causes Vkg-GFP to accumulate in the basal ER. The dashed line marks the apical surface. Experiments performed at stages 7–8. Scale bars represent 10 μm.

See also Figure S2.

follicle cells also produces round eggs (Figure 1D). We now refer to this mutation as $Plod^{N26\text{-}5}$.

Plod is an ER-resident enzyme that co- and posttranslationally modifies lysine residues on Col IV α chains (Myllylä et al., 2007). Previous work in *Drosophila* and other organisms has shown that Plod depletion leads to Col IV retention in the ER (Bunt et al., 2011; Norman and Moerman, 2000; Rautavuoma et al., 2004; Schneider and Granato, 2006; Sipilä et al., 2007). *Drosophila* have only one Col IV isoform, in which the α1 and α2 chains are Collagen gene at 25C (Cg25C) and Viking (Vkg), respectively (Natzle et al., 1982; Yasothornsrikul et al., 1997). To determine whether Col IV is retained in the ER of $Plod^{N26\text{-}5}$ cells, we used a GFP protein trap in the *vkg* locus (Vkg-GFP) (Buszczak et al., 2007). When wild-type follicle cells are viewed along their apical-basal axes, Vkg-GFP is typically only visible within the BM (Figure 1E). As expected, $Plod^{N26\text{-}5}$ follicle cells show intracellular Vkg-GFP accumulation, as well as reduced Vkg-GFP in the BM. However, we were surprised to find that the intracellular Col IV is always located near the basal surface, whereas the distribution of KDEL ER-retention signal and the ER membrane dye ER-tracker both reveal that this organelle extends throughout the cytoplasm (Figures 1E, 1F, S1C, and S1D). By performing transmission electron microscopy (TEM) on follicle cells expressing *Plod-RNAi*, we found that the ER structure is normal except for unusually distended basal ER cisternae, where the Col IV is presumably trapped (Figure 1G). These data indicate that Col IV accumulates in a basal ER compartment in Plod-depleted cells.

BM Proteins Are Locally Synthesized in a Basal ER Compartment

The pattern of Col IV accumulation in $Plod^{N26\text{-}5}$ cells led us to hypothesize that Col IV may be synthesized near the basal surface. Indeed, ~70% of *Cg25C* and *vkg* mRNAs localize to the basal half of the cytoplasm, making it likely that the Col IV α chains are translated directly into the basal ER (Figures 2A, 2B, and S2A). Col IV protein is also basally enriched in wild-type cells (Figures S2B and S2C). Plod and Prolyl-4-hydroxylase-α EFB (PH4αEFB) enzymes modify Col IV α chains as they are translocated across the ER membrane (Myllyharju and Kivirikko, 2004). Significantly, the mRNAs for these proteins show a similar localization (Figures 2C, 2D, and S2A). Moreover, *PH4αEFB-RNAi* causes Col IV to become trapped in the basal ER, similar to loss of Plod (Figures 2E and S2D). Basal enrichment is not a general property of follicle cell mRNAs, as we and others have also identified ER-associated transcripts that localize to the apical cytoplasm (Horne-Badovinac and Bilder, 2008; Konsolaki and Schüpbach, 1998; Li et al., 2008). Together, these data indicate that Col IV is predominantly synthesized in a basal ER compartment in wild-type follicle cells.

Col IV production in the basal ER raises the possibility that local synthesis promotes polarized secretion to the BM. Unlike mammalian cells in which the Golgi often forms a singular organelle called the Golgi ribbon, *Drosophila* cells have a distributed system in which small Golgi clusters are found throughout the cytoplasm. Each cluster is associated with a transitional ER (tER) site, from which newly synthesized proteins exit the ER. This organization of the early secretory pathway makes it possible for proteins synthesized in a subregion of the ER to be dispatched through the tER-Golgi units closest to the targeted plasma membrane (Kondylis et al., 2009; Kondylis and Rabouille, 2009).

To determine whether Col IV exits the ER from the basal region where it is synthesized, we investigated the function of the Tango1 cargo receptor, which helps package Col IV into enlarged Golgi-bound vesicles (Saito et al., 2009; Wilson et al., 2011). For these studies, we raised an antibody against Tango1 and validated its specificity (Figure S3A). This protein localizes to ~90% of tER-Golgi units, as shown by colocalization with the CopII-associated GTPase Sar1 and the *cis*-Golgi marker GM130 (Figures 3A, S3B, and S3C). Although tER-Golgi units are evenly distributed along the apical-basal axis, the Tango1 signal is much stronger at basal tER sites (Figures 3A, S3B, and S3D). Significantly, Vkg-GFP also accumulates at the basal Tango1-positive tER sites in wild-type cells (Figure 3B), and *Tango1-RNAi* causes most Vkg-GFP to become trapped in the basal ER (Figures 3C and S3E). It therefore appears that most Col IV exits the ER though basally-localized tER-Golgi units.

We next asked whether other BM proteins are also synthesized in the basal ER. Quantification of intracellular laminin and

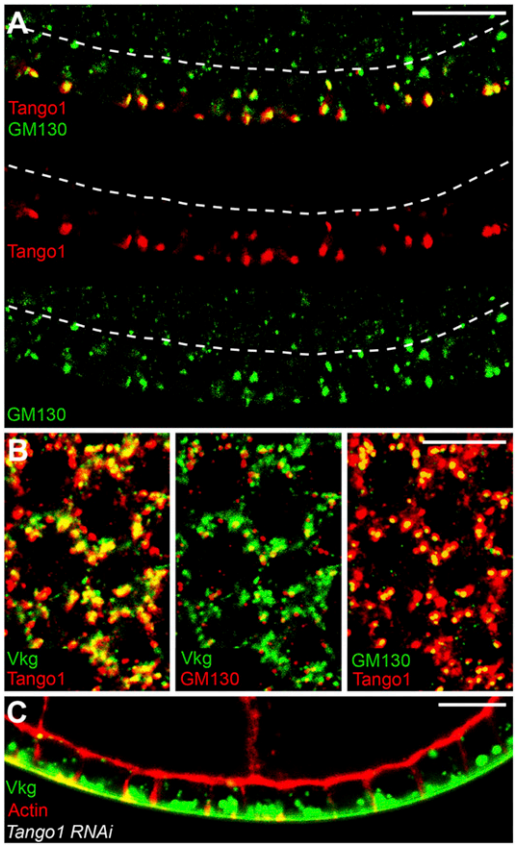

Figure 3. Tango1 Mediates Col IV ER Exit Predominantly at Basal tER Sites

(A) Tango1 is strongly enriched at basal tER-Golgi units, as indicated by the *cis*-Golgi marker, GM130. Dashed lines mark the apical surface.

(B) An optical section through the basal cytoplasm showing colocalization between Tango1, GM130, and Vkg-GFP.

(C) *Tango1-RNAi* causes Vkg-GFP to accumulate in the basal ER. Experiments performed at stages 7–8. Scale bars represent 10 μm.

See also Figure S3.

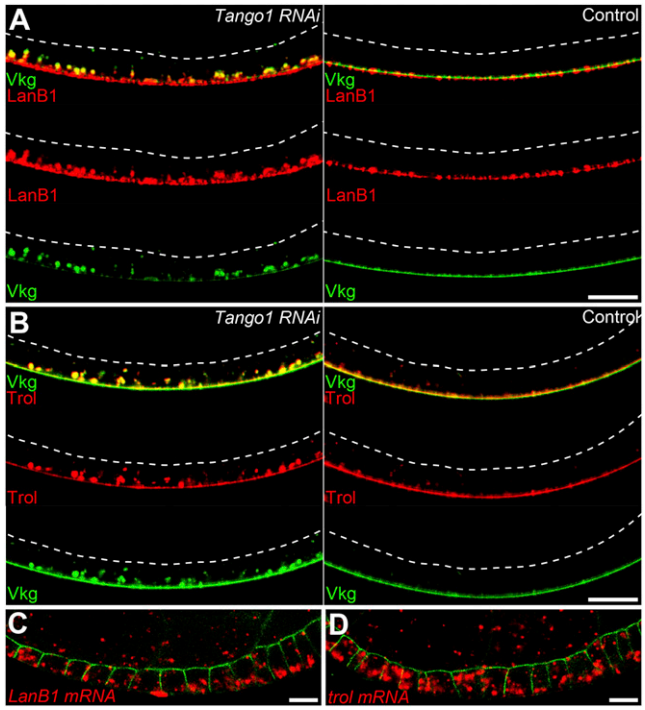

Figure 4. Laminin and Trol Are Also Enriched in the Basal Cytoplasm

(A and B) *Tango1-RNAi* causes LanB1 (A) and Trol (B) to accumulate in the basal ER with Vkg-GFP. Dashed lines mark the apical surface.

(C) *LanB1* mRNA is basally enriched. α-Spectrin marks the apical and lateral epithelial surfaces.

(D) *trol* mRNA does not show a basal bias. α-Spectrin marks the apical and lateral epithelial surfaces. Experiments performed at stages 7–8. Scale bars represent 10 μm.

See also Figure S4.

perlecan (Trol in *Drosophila*) levels revealed that these proteins are also enriched in the basal cytoplasm (Figures S4A–S4D). Moreover, *Tango1-RNAi* causes both proteins to accumulate in the basal ER with Col IV (Figures 4A and 4B). To investigate whether these proteins are translated directly into the basal ER, we again examined mRNA localization. Similar to the Col IV-encoding mRNAs, *Laminin B1* transcripts are enriched in the basal cytoplasm (Figures 4C and S4E). Conversely, *trol* transcripts show no basal bias (Figures 4D and S4E), suggesting that this protein's enrichment in the basal ER occurs by a separate mechanism. These data suggest that Laminin is also synthesized in the basal ER, and that other BM proteins may exit with Col IV through Tango1-positive tER sites.

Crag Regulates Rab10 to Promote Polarized BM Secretion

If BM proteins predominantly traffic through basal tER-Golgi units, how then do they reach the basal cell surface? Rab proteins are small GTPases that function as master regulators of intracellular membrane traffic (Hutagalung and Novick, 2011). Using a transgenic collection of YFP-tagged Rabs (Zhang et al., 2007), we found that Rab10 has an intriguing localization pattern. In addition to general cytoplasmic staining, there is a strong YFP-Rab10 signal near the basal follicle cell surface (Figures 5A and S5A). Significantly, *Rab10-RNAi* causes large BM proteins like Col IV, perlecan and laminin to accumulate on both the basal and apical surfaces (Figures 5B–5D); this phenotype is seen to a lesser extent with the smaller BM protein nidogen (Figure S5B). In contrast, *Rab10-RNAi* has no effect on the localization of four other proteins that normally undergo polarized trafficking in the follicle cells (Figures 5E, 5G, and S5C). The basal enrichment of BM-encoding mRNAs and Tango1 is also normal under these conditions (Figures S5D–S5F). Thus, Rab10 is required downstream of the basal bias in BM synthesis to ensure that BM proteins are delivered exclusively to the basal cell surface.

The apical accumulation of BM proteins in Rab10-depleted cells is remarkably similar to the phenotype first described for *Crag* (Denef et al., 2008). We therefore investigated the relationship between these two proteins. Although Crag is broadly distributed along the follicle cell apical-basal axis (Denef et al., 2008), an optical section near the basal surface revealed that Crag and Rab10 colocalize in this region (Figures 6A and S6A).

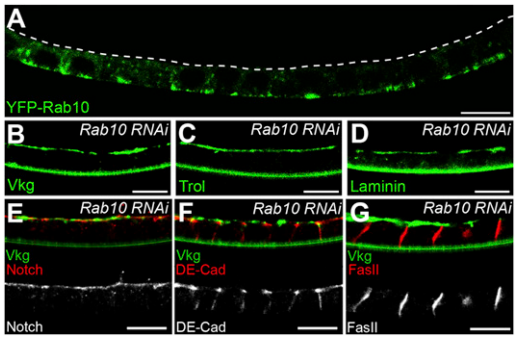

Figure 5. Rab10 Promotes Polarized BM Secretion

(A) YFP-Rab10 is enriched near the basal follicle cell surface. The dashed line marks the apical surface.

(B–D) *Rab10-RNAi* mis-targets Col IV (Vkg-GFP) (B), Perlecan (Trol-GFP) (C), and laminin to the apical surface (D).

(E–G) *Rab10-RNAi* does not affect the localization of apical (Notch) (E), junctional (DE-Cadherin) (F), or lateral (FasII) transmembrane proteins (G). Rab10 knockdown is shown by apical Vkg-GFP. Experiments performed at stages 7–8, except (C) and (D), which are stage 9. Scale bars represent 10 μm.

See also Figure S5.

Moreover, in *Crag*^{GG43} follicle cell clones, the strong YFP-Rab10 signal largely disappears from the basal surface, and is redistributed to the apical cytoplasm (Figures 6B and S6B). *Rab10* mRNA shows a 60% basal enrichment, which is unchanged under *Crag-RNAi* (Figure S6C). It therefore appears that Crag is required for the posttranslational targeting of Rab10 to structures near the basal cell surface.

Recently, Crag's mammalian homologs have been shown to function as highly specific Rab10 guanine nucleotide exchange factors (GEFs) in vitro (Yoshimura et al., 2010). Rab proteins with mutations that block GTP binding are thought to act as dominant negatives, in part, by sequestering GEFs (Li and Stahl, 1993; Stenmark et al., 1994). If Crag is a Rab10 GEF in this system, overexpressing Crag together with a Rab10.T23N dominant negative transgene may suppress the dominant negative phenotype (Zhu et al., 2007). Similar to *Rab10-RNAi*, expression of *UAS-Rab10.T23N* causes Vkg-GFP to accumulate on the apical surface (Figure 6E). Importantly, coexpressing *UAS-HA-Crag* with *UAS-Rab10.T23N* rescues this defect (Figures 6C–6F). We have also confirmed that Crag and Rab10 physically interact through coimmunoprecipitation experiments (Figure S6D). Combined with the mammalian data, these results argue that Crag functions as a Rab10 GEF to promote polarized BM secretion.

Denn domain proteins can bind multiple Rabs through interactions both within and outside their GEF domain. Crag has been previously shown to colocalize with Rab5 and Rab11 in the follicle cells (Denef et al., 2008). Rab5 depletion has no effect on polarized BM secretion (Figure S6E). Interestingly, however, we did observe Rab11 punctae interspersed with the Crag and Rab10 signals in the basal cytoplasm (Figure S6F). To investigate whether Rab11 regulates BM secretion, we followed Vkg-GFP localization under a series of RNAi conditions. Unlike the situation with *Rab10-RNAi* (Figures 5B and 6I), the Vkg-GFP localization in Rab11-depleted cells is similar to wild-type controls (Figures 6G and 6H). However, when we simultaneously

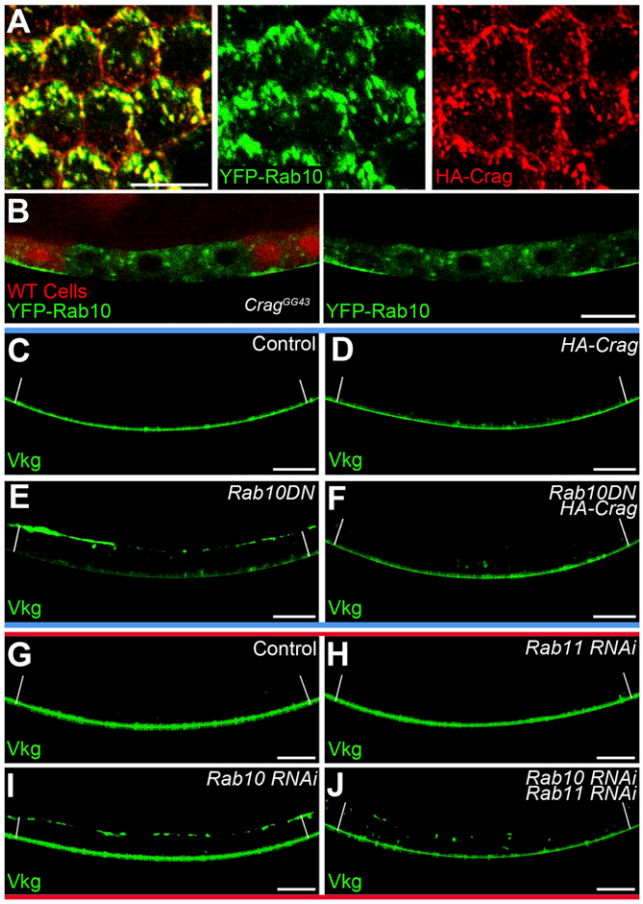

Figure 6. Crag Regulates Rab10 during Polarized BM Secretion

(A) Optical section near the basal surface showing YFP-Rab10 and HA-Crag colocalization.

(B) A *Crag*^{GG43} follicle cell clone shows a redistribution of YFP-Rab10 away from the basal surface.

(C and D) Interaction between *UAS-HA-Crag* and *UAS-Rab10.T23N*. Vkg-GFP localization is normal in wild-type (C) and *UAS-HA-Crag* (D) follicle cells. White lines extend between the apical and basal epithelial surfaces.

(E) Interaction between *UAS-HA-Crag* and *UAS-Rab10.T23N*. A *UAS-Rab10.T23N* dominant negative transgene causes Vkg-GFP to accumulate on the apical surface. A YFP on Rab10.T23N contributes to the fluorescent signal in the cytoplasm. White lines extend between the apical and basal epithelial surfaces.

(F) Interaction between *UAS-HA-Crag* and *UAS-Rab10.T23N*. Coexpression of *UAS-HA-Crag* with *UAS-Rab10.T23N* suppresses this phenotype. A YFP on Rab10.T23N contributes to the fluorescent signal in the cytoplasm. White lines extend between the apical and basal epithelial surfaces.

(G and H) Interaction between *Rab10-RNAi* and *Rab11-RNAi*. Vkg-GFP localization is normal in (G) wild-type and (H) Rab11-depleted cells. White lines extend between the apical and basal epithelial surfaces.

(I) Interaction between *Rab10-RNAi* and *Rab11-RNAi*. Rab10 depletion causes Vkg-GFP to accumulate on the apical surface. White lines extend between the apical and basal epithelial surfaces.

(J) Interaction between *Rab10-RNAi* and *Rab11-RNAi*. Codepletion of Rab10 and Rab11 eliminates the apical Vkg-GFP and increases the cytoplasmic signal. White lines extend between the apical and basal epithelial surfaces. Experiments performed at stages 7–8. Scale bar represents 10 μm.

See also Figure S6.

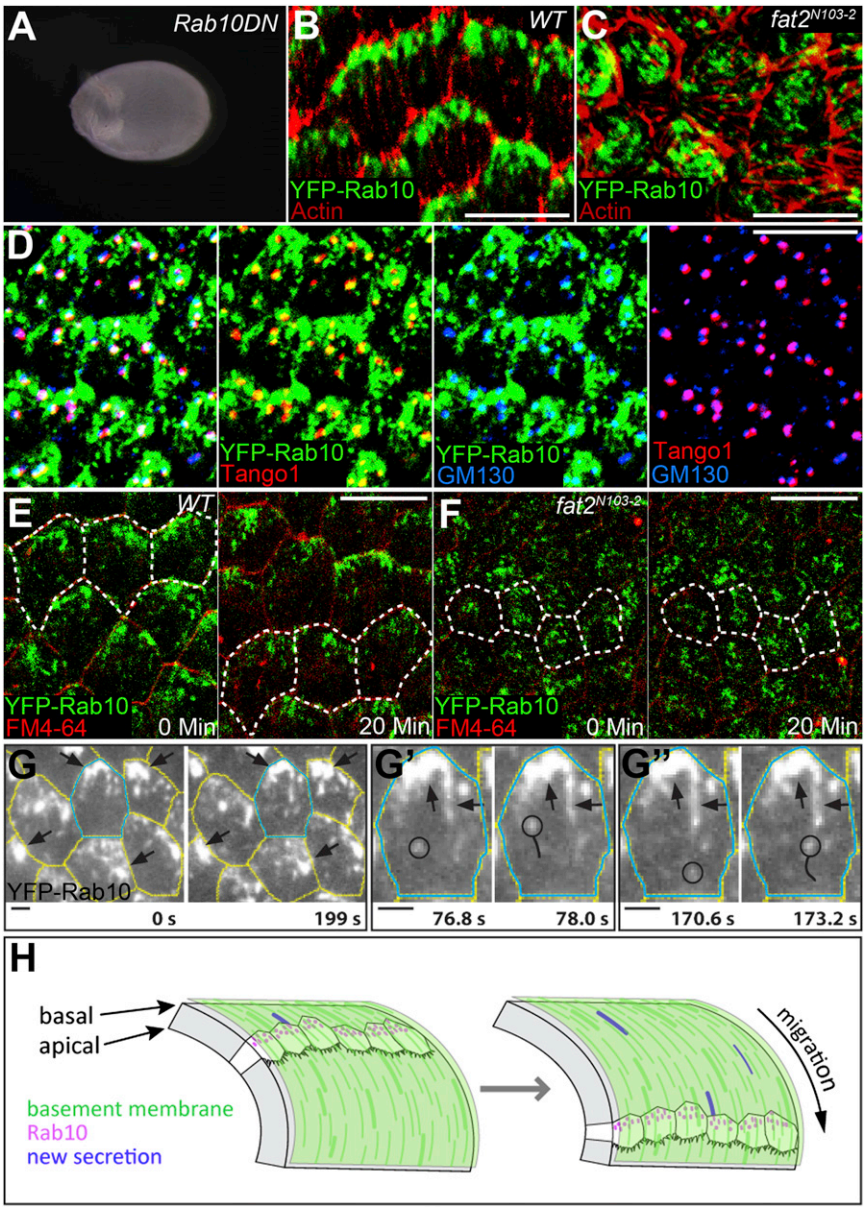

Figure 7. The BM Exocytic Machinery Is Planar Polarized at the Basal Epithelial Surface

(A) Rab10.T23N expression produces round eggs.

(B) YFP-Rab10 is planar polarized at the level of the basal actin filaments. Scale bar represents 10 μm.

(C) YFP-Rab10's planar polarization is lost in *fat2*$^{N103-2}$ epithelia. Scale bar represents 10 μm.

(D) Tango1 and GM130 are also planar polarized and partially overlap with YFP-Rab10. Scale bar represents 10 μm.

(E) Live imaging reveals that YFP-Rab10 is enriched at the trailing edge of each migrating cell. Scale bar represents 10 μm. FM4-64 marks cell membranes. Dashed lines mark the same three to four cells at each time point.

(F) *fat2*$^{N103-2}$ epithelia fail to migrate and YFP-Rab10 is mispolarized. Scale bar represents 10 μm. FM4-64 marks cell membranes. Dashed lines mark the same three to four cells at each time point.

(G–G″) TIRF microscopy reveals that larger Rab10-positive structures are largely immobile (arrows), whereas smaller Rab10-positive structures (circles in G′ and G″) move rapidly through the cytoplasm. Scale bars represent 2 μm.

(H) Speculative model for how planar polarization of BM secretion would synergize with follicle cell migration to create the unusual BM fibrils associated with egg chamber elongation. Illustration adapted from Bilder and Haigo (2012). Experiments performed at stages 7–8.

See also Figure S7 and Movies S1, S2, and S3.

depleted Rab10 and Rab11, Vkg-GFP was no longer found on the apical surface, but often showed a punctate intracellular distribution, in addition to its BM localization (Figure 6J). This phenotype was also observed with simultaneous depletion of Crag and Rab11 (Figures S6G–S6J). We conclude that Rab11 does not regulate BM secretion under normal conditions, but that in the absence of Crag or Rab10, BM proteins are inappropriately targeted to the apical surface through a Rab11-dependent mechanism.

Planar Polarization of the BM Exocytic Machinery during Egg Chamber Elongation

All experiments described above were performed during oogenic stages 6–8, which is the peak period of Col IV production in the egg chamber (Haigo and Bilder, 2011). Significantly, this is also the time when planar polarization of the follicle cell epithelium first drives egg chamber elongation. We noticed that Rab10.T23N expression in the follicle cells produces round eggs (Figure 7A). Moreover, YFP-Rab10 shows a striking planar polarization at the basal epithelial surface, when viewed at the level of the basal actin filaments (Figure 7B). Tango1, GM130, and the translocon protein Sec61α are also planar polarized (Figures 7D, S7A, and S7B). Consistent with Rab10's role in mediating late stages of protein traffic to the plasma membrane (Cao et al., 2008; Chen et al., 2012; Sano et al., 2007; Schuck et al., 2007), most of the YFP-Rab10 signal lies between the Tango1-positive tER-Golgi units and a basal region of the lateral plasma membrane (compare Figure 7D with 7B and 7E). Rab10 also partially overlaps with the tER-Golgi units (Figure 7D), but is not required for their planar polarization (Figure S7B). This unexpected positioning of the BM exocytic machinery suggests that BM deposition may be polarized along both the apical-basal and planar axes during egg chamber elongation.

How does Rab10 become localized along the planar axis? The atypical cadherin Fat2 is a key regulator of follicle cell planar polarity (Viktorinová et al., 2009). In *fat2*$^{N103-2}$ epithelia, YFP-Rab10 is polarized normally along the apical-basal axis,

but is mislocalized within the epithelial plane (Figures 7C, S7C, and S7D). This effect is posttranslational, as *Rab10* mRNA is not polarized along the planar axis (Figure S7E). Interestingly, this pattern is the opposite of Crag loss of function, where Rab10's apical-basal polarization is disrupted, but the protein still present at the basal surface is planar polarized (Figures 6B, S6B, and S7F). Thus, Rab10's polarization along the apical-basal and planar axes is controlled by two different mechanisms, one requiring Crag and the other requiring Fat2.

Follicle cell planar polarity is intimately linked with a directed epithelial migration that creates fibril-like structures in the BM. Live imaging of wild-type epithelia revealed that the intense YFP-Rab10 signal corresponds to the trailing edge of each migrating cell (Figure 7E; Movie S1). Conversely, $fat2^{N103\text{-}2}$ epithelia do not migrate, and BM structure is highly disrupted (Figures 7F and S7G; Movie S2). Near-total internal reflection fluorescence (TIRF) imaging (Konopka and Bednarek, 2008; Tokunaga et al., 2008) of wild-type cells at higher temporal resolution shows that the large, Rab10-positive structures at the trailing edge are surprisingly stable (on the order of minutes), whereas smaller Rab10-positive structures move at speeds of up to 1 μm/s through the basal cytoplasm (Figure 7G; Movie S3). Although we do not yet know the identity of these Rab10-positive compartments, these observations suggest that newly synthesized BM proteins are secreted from the trailing edge of each follicle cell as it migrates, which may have important implications for BM remodeling during elongation morphogenesis.

DISCUSSION

The BM is essential for epithelial structure and morphogenesis; yet little is known about how the component proteins are secreted to the basal surface, or how this process is regulated during development. Here, we have shown that the synthesis and trafficking of BM proteins is largely restricted to the basal cytoplasm in the *Drosophila* follicle cells. We have also identified Rab10 as a key regulator of polarized BM secretion, and shown that Crag likely functions as a Rab10 GEF. Surprisingly, the BM exocytic machinery shows a striking planar polarity at the basal epithelial surface, specifically during the time when the BM is being remodeled to promote egg chamber elongation. We therefore propose that spatial control of BM production along two tissue axes may promote exocytic efficiency, BM remodeling, and organ morphogenesis.

The polarized deposition of the two major BM components, Col IV and laminin, appears to begin with the targeting of their transcripts to the basal cytoplasm. For mRNA localization to enhance polarized membrane traffic requires that the cell have distributed tER-Golgi units, as opposed to a single Golgi ribbon (Kondylis et al., 2009; Kondylis and Rabouille, 2009). With this modular organization, localized mRNAs can be translated into a subregion of the ER, and newly synthesized proteins quickly dispatched through the tER-Golgi units closest to the target cell surface. Elegant studies in *Drosophila* have documented the use of this strategy for the polarized secretion of the TGFα homolog Gurken in the oocyte, and for the apical secretion of Wingless in the embryo (Herpers and Rabouille, 2004; Simmonds et al., 2001). Moreover, the targeting of mRNAs encoding secreted and transmembrane proteins to neuronal dendrites containing Golgi outposts (structures analogous to tER-Golgi units) suggests that this distributed exocytic program is conserved in at least some vertebrate cells (Ramírez and Couve, 2011). We propose that the basal targeting of the Col IV- and laminin-encoding mRNAs may similarly enhance the delivery of these proteins to the basal surface.

The local synthesis of BM components may also address several challenges that these complex proteins pose to the ER. For example, Col IV requires dedicated machinery to mediate both trimer formation and ER exit. Concentrating these functions into a smaller ER region is therefore likely to increase Col IV biosynthetic efficiency. We have shown that the mRNAs encoding Plod and PH4αEFB are also enriched in the basal cytoplasm, and that loss of either protein causes Col IV to accumulate in the basal ER. Tango1 function is also higher at basal ER exit sites. Interestingly, the ECM component Aggrecan is synthesized in a restricted ER region in avian chondrocytes (Vertel et al., 1989). Thus, ER compartmentalization may be a conserved strategy for ECM biosynthesis.

Although local synthesis likely facilitates polarized BM secretion, additional downstream mechanisms are required to restrict protein delivery to the basal surface. The first evidence for this regulation came from Denef et al. (2008), who showed that loss of Crag causes BM proteins to accumulate on both the basal and apical follicle cell surfaces. The presence of the DENN domain made it likely that Crag was a direct regulator of polarized membrane traffic. Consistent with this notion, Crag localized to Rab5- and Rab11-positive endosomes, and along the apical and lateral plasma membranes (Denef et al., 2008). However, the diversity of the protein's distribution made it difficult to pinpoint Crag's function in polarized BM secretion.

Here, we have identified Rab10 as a second critical component in this system. Importantly, this protein shows a more restricted localization, with the strongest Rab10 signal being tightly associated with the basal cell surface. Crag colocalizes with Rab10 in this region and is required for Rab10's basal enrichment. Moreover, Rab10 interacts with Crag both genetically and physically, and Rab10 depletion phenocopies *Crag*'s BM defect. Given that Crag's mammalian homologs function as Rab10 GEFs in vitro (Yoshimura et al., 2010), we now propose that Crag functions as a Rab10 GEF in vivo to control polarized BM secretion.

It is likely, however, that Crag also has Rab10-independent functions. For instance, *Crag* mutant cells show defects in apical-basal polarity (Denef et al., 2008), whereas Rab10-depleted cells do not (data not shown). This phenotypic difference could be due to incomplete Rab10 knockdown, but it is also consistent with Crag regulating more than one trafficking pathway. DENN domain proteins can bind multiple Rabs through interactions outside their GEF domain (Marat et al., 2011). Because Crag also colocalizes with Rab5 and Rab11, both of which are required for follicle cell apical-basal polarity (Lu and Bilder, 2005; Xu et al., 2011), Crag may play a second role with these proteins controlling epithelial architecture.

How then does Rab10 control polarized BM secretion? We have shown that Rab10 has a complex distribution in the basal cytoplasm, where it associates both with Tango1-positive tER-Golgi units and the plasma membrane. Rab10 is a known

exocytic regulator in multiple organisms and cell types; however, the exact compartment(s) to which it localizes vary with cargo and cell polarization state (Babbey et al., 2006, 2010; Chen et al., 2006; Sano et al., 2007; Schuck et al., 2007; Wang et al., 2011). A recent proteomic analysis in MDCK cells found Rab10 on exocytic vesicles bound for a basal region of the lateral plasma membrane (Cao et al., 2008). We propose that Rab10 may localize to similarly targeted exocytic vesicles in the follicle cells. Interestingly, Rab10 is not absolutely required for basal secretion, as a significant fraction of BM proteins do reach the basal surface when Rab10 is depleted. However, it is required to stop BM proteins from taking an alternate, Rab11-dependent route to the apical surface. Thus, local synthesis may provide sufficient information for the basal targeting of some BM vesicles, but Rab10 is required to ensure robust polarized secretion.

In addition to identifying mechanisms directing BM secretion to the basal surface, this work also provides a strong foundation for future studies of BM remodeling during egg chamber elongation. We have shown that the BM exocytic machinery is enriched at the trailing edge of each migrating follicle cell in a Fat2-dependent manner, a surprising observation given that many migrating cells orient their Golgi toward the front (Sütterlin and Colanzi, 2010; Yadav and Linstedt, 2011). It has been proposed, however, that the entire purpose of follicle cell migration is to create the unusual fibril-like structures in the BM that promote egg chamber elongation (Haigo and Bilder, 2011). We have not yet identified the exact location where BM proteins exit the cell; however, Rab10's known function as a late exocytic regulator evokes the following model. We envision that newly synthesized BM proteins are quickly transported from basal tER-Golgi units to the trailing plasma membrane through a Rab10-dependent mechanism. Planar polarized secretion then synergizes with cell movement to produce the fibril-like structures in the BM (Figure 7H). Whether Rab10 directly regulates planar secretion is not yet clear, as the BM material that reaches the basal surface under Rab10 depletion still shows the fibril-like morphology (data not shown). However, incomplete depletion and/or partial redundancy with closely related Rabs may obscure this aspect of Rab10's function (Schuck et al., 2007; Shi et al., 2010). The follicle cells thus provide a powerful system to investigate the dynamic regulation of BM secretion and remodeling during organ morphogenesis.

EXPERIMENTAL PROCEDURES

Drosophila Genetics

Follicle cell clones were generated using *e22c-Gal4* to drive expression of the FLP recombinase. UAS transgenes were expressed with *TubP-Gal4* or *traffic jam-Gal4* (*tj-Gal4*) for full follicle cell expression, or *hs-FLP; Act5c≫Gal4* for clones. Most lines are from the Bloomington *Drosophila* stock center, with exceptions listed below. RNAi lines for Plod, Tango1, and Rab5 are from the Vienna *Drosophila* RNAi Center. *Rab11-RNAi* is from Satoh et al. (2005). *tj-Gal4* (NP1624) is from the *Drosophila* Genetic Resource Center, Kyoto. *vkg-GFP* (CC00791), *trol-GFP* (CA06698), *Sar1-GFP* (CA07674), and *Sec61α-GFP* (CC00735) are from Buszczak et al. (2007). $Crag^{GG43}$, *FRT19A*, and *UAS-HA-Crag* are from Denef et al. (2008). $fat2^{N103-2}$, *FRT80* is from Horne-Badovinac et al. (2012). w^{1118} typically served as a wild-type control. Most crosses were raised, and experiments performed at 25°C. Full genotypes for each experiment and unusual temperature conditions can be found in Supplemental Experimental Procedures.

Fluorescent In Situ Hybridization

For probe synthesis, a single coding exon was PCR-amplified from w^{1118} genomic DNA, using a reverse primer with the T7 promoter sequence (see Supplemental Experimental Procedures). The PCR products were purified by Qiaquick gel purification (QIAGEN) and antisense probes synthesized using a DIG RNA labeling kit (Roche). For *trol* mRNA, we used a probe against *GFP* on tissue expressing the *Trol-GFP* protein trap. The antisense *GFP* probe was synthesized from the *pBS-eGFPA* vector, by linearizing with KpnI and transcribing with the T7 polymerase. Probes were detected using an HRP-conjugated sheep anti-DIG antibody (1:1,000, Roche), followed by TSA Cyanine 3 staining (Perkin Elmer). Ovaries were then stained with mouse anti-α-Spectrin (1:50, DSHB, concentrate). Samples were mounted in SlowFade Antifade (Invitrogen). Images were obtained using a Zeiss LSM 510 confocal microscope and processed with Photoshop.

Immunofluorescence and Staining

Ovaries were dissected in S2 medium and fixed for 15 min in 4% EM-grade formaldehyde (Polysciences). Antibody stains were performed in PBS with 0.1% Triton, and detected using Alexa Fluor-conjugated secondary antibodies (1:200, Invitrogen). TRITC-Phalloidin (1:200, Sigma) or AlexaFluor-647 Phalloidin (1:50, Invitrogen) were used to label cell cortices. ER-Tracker Red (Invitrogen) was diluted in PBS with 4% EM-grade formaldehyde (Polysciences) and the staining reaction was incubated at 37°C for 20 min. Egg chambers were mounted in SlowFade Antifade (Invitrogen) and visualized using a Zeiss LSM 510 confocal microscope. Commercial antibodies include mouse α-KDEL (10C3, 1:25, Calbiochem), rabbit α-GM130 (1:200, Abcam), rabbit α-HA (1:200, Rockland), mouse α-Rab11 (1:20, BD Biosciences), and rabbit α-LanB1 (1:100, Abcam). DSHB antibodies include mouse α-Notch (C458.2H,1:20), rat α-DE-Cadherin (DCAD2, 1:20), mouse α-FasII (1D4, 1:10), and mouse α-FasIII (7G10, 1:10). Rabbit α-laminin (1:100), rabbit α-Pcan (1:1,000), and rabbit α-nidogen (1:1,000) are from Fessler et al. (1987), Friedrich et al. (2000), and Wolfstetter et al. (2009), respectively. Guinea pig α-Tango1 (1:200) is from this study.

Live Imaging

Live imaging of follicle cell migration was performed as described (Prasad et al., 2007), with the following modifications. Dissected egg chambers were placed onto a pad of 0.4% NuSieve GTG low melt agarose (Lonza) in live imaging medium, and follicle cell membranes were marked with 6.6 μM FM4-64FX (Invitrogen). The coverslip was cushioned with vacuum grease at each corner, and then sealed with halocarbon oil 27 (Sigma). Confocal movies were taken on a Zeiss LSM 510 microscope, and processed using LSM image browser. TIRF movies were taken on an Olympus IX-50 microscope equipped with an iXon EMCCD camera (Andor) and a 100× objective fitted with through-the-objective TIRF illumination, and processed using ImageJ.

SUPPLEMENTAL INFORMATION

Supplemental Information includes seven figures, three movies, and Supplemental Experimental Procedures and can be found with this article online at http://dx.doi.org/10.1016/j.devcel.2012.12.005.

ACKNOWLEDGMENTS

Trudi Schüpbach, Lisa Fessler, Stefan Baumgartner, and Anne Holz generously provided reagents. We are grateful to Amanda Neisch for help with antibody production, Pam Vanderzalm for advice on coIPs, Guillermina Ramirez-San Juan for MATLAB assistance, and Nick Badovinac for illustrations. We also thank Chip Ferguson, Ben Glick, Lucy O'Brien, and members of the Horne-Badovinac laboratory for comments on the manuscript. This work was supported by National Science Foundation predoctoral fellowships to D.W.L. and A.J.I., as well as a Basil O'Connor Starter Scholar Award (5-FY10-50) from the March of Dimes and NIH grant (R01GM094276) to S.H-B.

Received: June 26, 2012
Revised: October 16, 2012
Accepted: December 4, 2012
Published: January 28, 2013

REFERENCES

Arnaoutova, I., George, J., Kleinman, H.K., and Benton, G. (2012). Basement membrane matrix (BME) has multiple uses with stem cells. Stem Cell Rev. *8*, 163–169.

Babbey, C.M., Ahktar, N., Wang, E., Chen, C.C., Grant, B.D., and Dunn, K.W. (2006). Rab10 regulates membrane transport through early endosomes of polarized Madin-Darby canine kidney cells. Mol. Biol. Cell *17*, 3156–3175.

Babbey, C.M., Bacallao, R.L., and Dunn, K.W. (2010). Rab10 associates with primary cilia and the exocyst complex in renal epithelial cells. Am. J. Physiol. Renal Physiol. *299*, F495–F506.

Bilder, D., and Haigo, S.L. (2012). Expanding the morphogenetic repertoire: perspectives from the Drosophila egg. Dev. Cell *22*, 12–23.

Boll, W., Partin, J.S., Katz, A.I., Caplan, M.J., and Jamieson, J.D. (1991). Distinct pathways for basolateral targeting of membrane and secretory proteins in polarized epithelial cells. Proc. Natl. Acad. Sci. USA *88*, 8592–8596.

Bunt, S., Hooley, C., Hu, N., Scahill, C., Weavers, H., and Skaer, H. (2010). Hemocyte-secreted type IV collagen enhances BMP signaling to guide renal tubule morphogenesis in Drosophila. Dev. Cell *19*, 296–306.

Bunt, S., Denholm, B., and Skaer, H. (2011). Characterisation of the Drosophila procollagen lysyl hydroxylase, dPlod. Gene Expr. Patterns *11*, 72–78.

Buszczak, M., Paterno, S., Lighthouse, D., Bachman, J., Planck, J., Owen, S., Skora, A.D., Nystul, T.G., Ohlstein, B., Allen, A., et al. (2007). The Carnegie protein trap library: a versatile tool for Drosophila developmental studies. Genetics *175*, 1505–1531.

Cao, Z., Li, C., Higginbotham, J.N., Franklin, J.L., Tabb, D.L., Graves-Deal, R., Hill, S., Cheek, K., Jerome, W.G., Lapierre, L.A., et al. (2008). Use of fluorescence-activated vesicle sorting for isolation of Naked2-associated, basolaterally targeted exocytic vesicles for proteomics analysis. Mol. Cell. Proteomics *7*, 1651–1667.

Caplan, M.J., Stow, J.L., Newman, A.P., Madri, J., Anderson, H.C., Farquhar, M.G., Palade, G.E., and Jamieson, J.D. (1987). Dependence on pH of polarized sorting of secreted proteins. Nature *329*, 632–635.

Chen, C.C., Schweinsberg, P.J., Vashist, S., Mareiniss, D.P., Lambie, E.J., and Grant, B.D. (2006). RAB-10 is required for endocytic recycling in the Caenorhabditis elegans intestine. Mol. Biol. Cell *17*, 1286–1297.

Chen, Y., Wang, Y., Zhang, J., Deng, Y., Jiang, L., Song, E., Wu, X.S., Hammer, J.A., Xu, T., and Lippincott-Schwartz, J. (2012). Rab10 and myosin-Va mediate insulin-stimulated GLUT4 storage vesicle translocation in adipocytes. J. Cell Biol. *198*, 545–560.

Cohen, D., Müsch, A., and Rodriguez-Boulan, E. (2001). Selective control of basolateral membrane protein polarity by cdc42. Traffic *2*, 556–564.

De Almeida, J.B., and Stow, J.L. (1991). Disruption of microtubules alters polarity of basement membrane proteoglycan secretion in epithelial cells. Am. J. Physiol. *261*, C691–C700.

Denef, N., Chen, Y., Weeks, S.D., Barcelo, G., and Schüpbach, T. (2008). Crag regulates epithelial architecture and polarized deposition of basement membrane proteins in Drosophila. Dev. Cell *14*, 354–364.

Eastburn, D.J., and Mostov, K.E. (2010). Laying the foundation for epithelia: insights into polarized basement membrane deposition. EMBO Rep. *11*, 329–330.

Fata, J.E., Werb, Z., and Bissell, M.J. (2004). Regulation of mammary gland branching morphogenesis by the extracellular matrix and its remodeling enzymes. Breast Cancer Res. *6*, 1–11.

Fessler, L.I., Campbell, A.G., Duncan, K.G., and Fessler, J.H. (1987). Drosophila laminin: characterization and localization. J. Cell Biol. *105*, 2383–2391.

Friedrich, M.V., Schneider, M., Timpl, R., and Baumgartner, S. (2000). Perlecan domain V of Drosophila melanogaster. Sequence, recombinant analysis and tissue expression. Eur. J. Biochem. *267*, 3149–3159.

Fromme, J.C., and Schekman, R. (2005). COPII-coated vesicles: flexible enough for large cargo? Curr. Opin. Cell Biol. *17*, 345–352.

Gutzeit, H.O. (1990). The microfilament pattern in the somatic follicle cells of mid-vitellogenic ovarian follicles of Drosophila. Eur. J. Cell Biol. *53*, 349–356.

Gutzeit, H.O., Eberhardt, W., and Gratwohl, E. (1991). Laminin and basement membrane-associated microfilaments in wild-type and mutant Drosophila ovarian follicles. J. Cell Sci. *100*, 781–788.

Haigo, S.L., and Bilder, D. (2011). Global tissue revolutions in a morphogenetic movement controlling elongation. Science *331*, 1071–1074.

Herpers, B., and Rabouille, C. (2004). mRNA localization and ER-based protein sorting mechanisms dictate the use of transitional endoplasmic reticulum-golgi units involved in gurken transport in Drosophila oocytes. Mol. Biol. Cell *15*, 5306–5317.

Horne-Badovinac, S., and Bilder, D. (2008). Dynein regulates epithelial polarity and the apical localization of stardust A mRNA. PLoS Genet. *4*, e8.

Horne-Badovinac, S., Hill, J., Gerlach, G., 2nd, Menegas, W., and Bilder, D. (2012). A screen for round egg mutants in Drosophila identifies tricornered, furry, and misshapen as regulators of egg chamber elongation. G3 (Bethesda) *2*, 371–378.

Hutagalung, A.H., and Novick, P.J. (2011). Role of Rab GTPases in membrane traffic and cell physiology. Physiol. Rev. *91*, 119–149.

Jin, L., Pahuja, K.B., Wickliffe, K.E., Gorur, A., Baumgärtel, C., Schekman, R., and Rape, M. (2012). Ubiquitin-dependent regulation of COPII coat size and function. Nature *482*, 495–500.

Kalluri, R. (2003). Basement membranes: structure, assembly and role in tumour angiogenesis. Nat. Rev. Cancer *3*, 422–433.

Khoshnoodi, J., Pedchenko, V., and Hudson, B.G. (2008). Mammalian collagen IV. Microsc. Res. Tech. *71*, 357–370.

Kondylis, V., and Rabouille, C. (2009). The Golgi apparatus: lessons from Drosophila. FEBS Lett. *583*, 3827–3838.

Kondylis, V., Pizette, S., and Rabouille, C. (2009). The early secretory pathway in development: a tale of proteins and mRNAs. Semin. Cell Dev. Biol. *20*, 817–827.

Konopka, C.A., and Bednarek, S.Y. (2008). Variable-angle epifluorescence microscopy: a new way to look at protein dynamics in the plant cell cortex. Plant J. *53*, 186–196.

Konsolaki, M., and Schüpbach, T. (1998). Windbeutel, a gene required for dorsoventral patterning in Drosophila, encodes a protein that has homologies to vertebrate proteins of the endoplasmic reticulum. Genes Dev. *12*, 120–131.

Li, G., and Stahl, P.D. (1993). Structure-function relationship of the small GTPase rab5. J. Biol. Chem. *268*, 24475–24480.

Li, Z., Wang, L., Hays, T.S., and Cai, Y. (2008). Dynein-mediated apical localization of crumbs transcripts is required for Crumbs activity in epithelial polarity. J. Cell Biol. *180*, 31–38.

Lu, H., and Bilder, D. (2005). Endocytic control of epithelial polarity and proliferation in Drosophila. Nat. Cell Biol. *7*, 1232–1239.

Malhotra, V., and Erlmann, P. (2011). Protein export at the ER: loading big collagens into COPII carriers. EMBO J. *30*, 3475–3480.

Marat, A.L., Dokainish, H., and McPherson, P.S. (2011). DENN domain proteins: regulators of Rab GTPases. J. Biol. Chem. *286*, 13791–13800.

Mellman, I., and Nelson, W.J. (2008). Coordinated protein sorting, targeting and distribution in polarized cells. Nat. Rev. Mol. Cell Biol. *9*, 833–845.

Miner, J.H. (2011). Glomerular basement membrane composition and the filtration barrier. Pediatr. Nephrol. *26*, 1413–1417.

Miner, J.H., and Yurchenco, P.D. (2004). Laminin functions in tissue morphogenesis. Annu. Rev. Cell Dev. Biol. *20*, 255–284.

Mirouse, V., Christoforou, C.P., Fritsch, C., St Johnston, D., and Ray, R.P. (2009). Dystroglycan and perlecan provide a basal cue required for epithelial polarity during energetic stress. Dev. Cell *16*, 83–92.

Mirre, C., Cecchini, J.P., Le Parco, Y., and Knibiehler, B. (1988). De novo expression of a type IV collagen gene in Drosophila embryos is restricted to mesodermal derivatives and occurs at germ band shortening. Development *102*, 369–376.

Myllyharju, J., and Kivirikko, K.I. (2004). Collagens, modifying enzymes and their mutations in humans, flies and worms. Trends Genet. *20*, 33–43.

Myllylä, R., Wang, C., Heikkinen, J., Juffer, A., Lampela, O., Risteli, M., Ruotsalainen, H., Salo, A., and Sipilä, L. (2007). Expanding the lysyl

hydroxylase toolbox: new insights into the localization and activities of lysyl hydroxylase 3 (LH3). J. Cell. Physiol. *212*, 323–329.

Natzle, J.E., Monson, J.M., and McCarthy, B.J. (1982). Cytogenetic location and expression of collagen-like genes in Drosophila. Nature *296*, 368–371.

Norman, K.R., and Moerman, D.G. (2000). The let-268 locus of Caenorhabditis elegans encodes a procollagen lysyl hydroxylase that is essential for type IV collagen secretion. Dev. Biol. *227*, 690–705.

O'Brien, L.E., Jou, T.S., Pollack, A.L., Zhang, Q., Hansen, S.H., Yurchenco, P., and Mostov, K.E. (2001). Rac1 orientates epithelial apical polarity through effects on basolateral laminin assembly. Nat. Cell Biol. *3*, 831–838.

Pastor-Pareja, J.C., and Xu, T. (2011). Shaping cells and organs in Drosophila by opposing roles of fat body-secreted Collagen IV and perlecan. Dev. Cell *21*, 245–256.

Prasad, M., Jang, A.C., Starz-Gaiano, M., Melani, M., and Montell, D.J. (2007). A protocol for culturing Drosophila melanogaster stage 9 egg chambers for live imaging. Nat. Protoc. *2*, 2467–2473.

Ramírez, O.A., and Couve, A. (2011). The endoplasmic reticulum and protein trafficking in dendrites and axons. Trends Cell Biol. *21*, 219–227.

Rautavuoma, K., Takaluoma, K., Sormunen, R., Myllyharju, J., Kivirikko, K.I., and Soininen, R. (2004). Premature aggregation of type IV collagen and early lethality in lysyl hydroxylase 3 null mice. Proc. Natl. Acad. Sci. USA *101*, 14120–14125.

Rodriguez-Boulan, E., Kreitzer, G., and Müsch, A. (2005). Organization of vesicular trafficking in epithelia. Nat. Rev. Mol. Cell Biol. *6*, 233–247.

Saito, K., Chen, M., Bard, F., Chen, S., Zhou, H., Woodley, D., Polischuk, R., Schekman, R., and Malhotra, V. (2009). TANGO1 facilitates cargo loading at endoplasmic reticulum exit sites. Cell *136*, 891–902.

Sano, H., Eguez, L., Teruel, M.N., Fukuda, M., Chuang, T.D., Chavez, J.A., Lienhard, G.E., and McGraw, T.E. (2007). Rab10, a target of the AS160 Rab GAP, is required for insulin-stimulated translocation of GLUT4 to the adipocyte plasma membrane. Cell Metab. *5*, 293–303.

Satoh, A.K., O'Tousa, J.E., Ozaki, K., and Ready, D.F. (2005). Rab11 mediates post-Golgi trafficking of rhodopsin to the photosensitive apical membrane of Drosophila photoreceptors. Development *132*, 1487–1497.

Schneider, M., Khalil, A.A., Poulton, J., Castillejo-Lopez, C., Egger-Adam, D., Wodarz, A., Deng, W.M., and Baumgartner, S. (2006). Perlecan and Dystroglycan act at the basal side of the Drosophila follicular epithelium to maintain epithelial organization. Development *133*, 3805–3815.

Schneider, V.A., and Granato, M. (2006). The myotomal diwanka (lh3) glycosyltransferase and type XVIII collagen are critical for motor growth cone migration. Neuron *50*, 683–695.

Schuck, S., Gerl, M.J., Ang, A., Manninen, A., Keller, P., Mellman, I., and Simons, K. (2007). Rab10 is involved in basolateral transport in polarized Madin-Darby canine kidney cells. Traffic *8*, 47–60.

Shi, A., Chen, C.C., Banerjee, R., Glodowski, D., Audhya, A., Rongo, C., and Grant, B.D. (2010). EHBP-1 functions with RAB-10 during endocytic recycling in Caenorhabditis elegans. Mol. Biol. Cell *21*, 2930–2943.

Simmonds, A.J., dosSantos, G., Livne-Bar, I., and Krause, H.M. (2001). Apical localization of wingless transcripts is required for wingless signaling. Cell *105*, 197–207.

Sipilä, L., Ruotsalainen, H., Sormunen, R., Baker, N.L., Lamandé, S.R., Vapola, M., Wang, C., Sado, Y., Aszodi, A., and Myllylä, R. (2007). Secretion and assembly of type IV and VI collagens depend on glycosylation of hydroxylysines. J. Biol. Chem. *282*, 33381–33388.

Sorrosal, G., Pérez, L., Herranz, H., and Milán, M. (2010). Scarface, a secreted serine protease-like protein, regulates polarized localization of laminin A at the basement membrane of the Drosophila embryo. EMBO Rep. *11*, 373–379.

Stenmark, H., Parton, R.G., Steele-Mortimer, O., Lütcke, A., Gruenberg, J., and Zerial, M. (1994). Inhibition of rab5 GTPase activity stimulates membrane fusion in endocytosis. EMBO J. *13*, 1287–1296.

Sütterlin, C., and Colanzi, A. (2010). The Golgi and the centrosome: building a functional partnership. J. Cell Biol. *188*, 621–628.

Tokunaga, M., Imamoto, N., and Sakata-Sogawa, K. (2008). Highly inclined thin illumination enables clear single-molecule imaging in cells. Nat. Methods *5*, 159–161.

Urbano, J.M., Torgler, C.N., Molnar, C., Tepass, U., López-Varea, A., Brown, N.H., de Celis, J.F., and Martín-Bermudo, M.D. (2009). Drosophila laminins act as key regulators of basement membrane assembly and morphogenesis. Development *136*, 4165–4176.

Valastyan, S., and Weinberg, R.A. (2011). Tumor metastasis: molecular insights and evolving paradigms. Cell *147*, 275–292.

Venditti, R., Scanu, T., Santoro, M., Di Tullio, G., Spaar, A., Gaibisso, R., Beznoussenko, G.V., Mironov, A.A., Mironov, A., Jr., Zelante, L., et al. (2012). Sedlin controls the ER export of procollagen by regulating the Sar1 cycle. Science *337*, 1668–1672.

Vertel, B.M., Velasco, A., LaFrance, S., Walters, L., and Kaczman-Daniel, K. (1989). Precursors of chondroitin sulfate proteoglycan are segregated within a subcompartment of the chondrocyte endoplasmic reticulum. J. Cell Biol. *109*, 1827–1836.

Viktorinová, I., König, T., Schlichting, K., and Dahmann, C. (2009). The cadherin Fat2 is required for planar cell polarity in the Drosophila ovary. Development *136*, 4123–4132.

Wang, T., Liu, Y., Xu, X.H., Deng, C.Y., Wu, K.Y., Zhu, J., Fu, X.Q., He, M., and Luo, Z.G. (2011). Lgl1 activation of rab10 promotes axonal membrane trafficking underlying neuronal polarization. Dev. Cell *21*, 431–444.

Wang, X., Harris, R.E., Bayston, L.J., and Ashe, H.L. (2008). Type IV collagens regulate BMP signalling in Drosophila. Nature *455*, 72–77.

Wilson, D.G., Phamluong, K., Li, L., Sun, M., Cao, T.C., Liu, P.S., Modrusan, Z., Sandoval, W.N., Rangell, L., Carano, R.A., et al. (2011). Global defects in collagen secretion in a Mia3/TANGO1 knockout mouse. J. Cell Biol. *193*, 935–951.

Wolfstetter, G., Shirinian, M., Stute, C., Grabbe, C., Hummel, T., Baumgartner, S., Palmer, R.H., and Holz, A. (2009). Fusion of circular and longitudinal muscles in Drosophila is independent of the endoderm but further visceral muscle differentiation requires a close contact between mesoderm and endoderm. Mech. Dev. *126*, 721–736.

Xu, J., Lan, L., Bogard, N., Mattione, C., and Cohen, R.S. (2011). Rab11 is required for epithelial cell viability, terminal differentiation, and suppression of tumor-like growth in the Drosophila egg chamber. PLoS ONE *6*, e20180.

Yadav, S., and Linstedt, A.D. (2011). Golgi positioning. Cold Spring Harb. Perspect. Biol. *3*.

Yasothornsrikul, S., Davis, W.J., Cramer, G., Kimbrell, D.A., and Dearolf, C.R. (1997). Viking: identification and characterization of a second type IV collagen in Drosophila. Gene *198*, 17–25.

Yoshimura, S., Gerondopoulos, A., Linford, A., Rigden, D.J., and Barr, F.A. (2010). Family-wide characterization of the DENN domain Rab GDP-GTP exchange factors. J. Cell Biol. *191*, 367–381.

Yurchenco, P.D. (2011). Basement membranes: cell scaffoldings and signaling platforms. Cold Spring Harb. Perspect. Biol. *3*.

Zhang, J., Schulze, K.L., Hiesinger, P.R., Suyama, K., Wang, S., Fish, M., Acar, M., Hoskins, R.A., Bellen, H.J., and Scott, M.P. (2007). Thirty-one flavors of Drosophila rab proteins. Genetics *176*, 1307–1322.

Zhu, H., Zhu, G., Liu, J., Liang, Z., Zhang, X.C., and Li, G. (2007). Rabaptin-5-independent membrane targeting and Rab5 activation by Rabex-5 in the cell. Mol. Biol. Cell *18*, 4119–4128.

Developmental Cell, Volume *24*

Supplemental Information

A Rab10-Dependent Mechanism for Polarized Basement Membrane Secretion during Organ Morphogenesis

David W. Lerner, Darcy McCoy, Adam J. Isabella, Anthony P. Mahowald, Gary F. Gerlach, Thymur A. Chaudhry, and Sally Horne-Badovinac

INVENTORY OF SUPPLEMENTAL INFORMATION

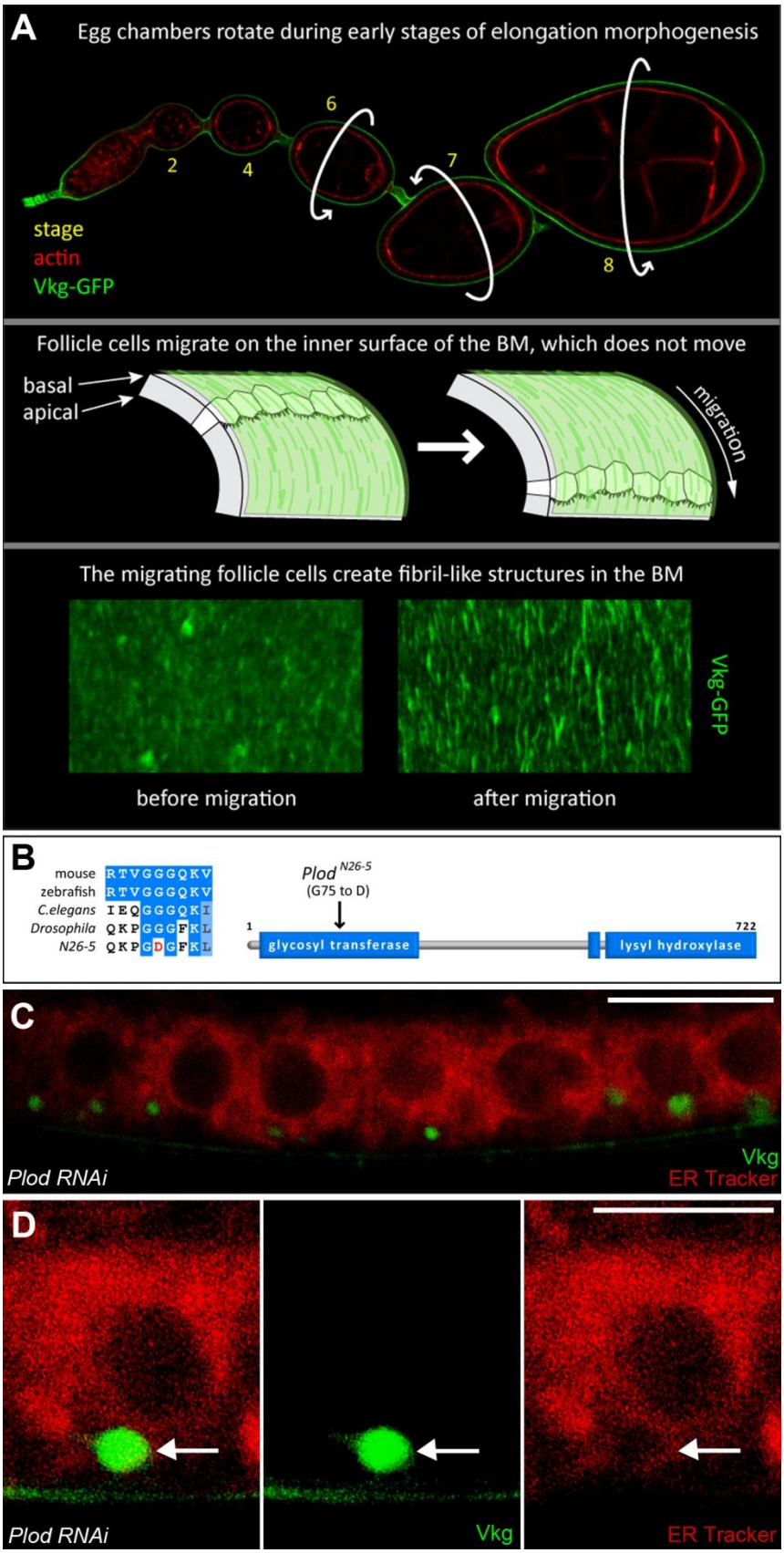
A
Egg chambers rotate during early stages of elongation morphogenesis
2
4
6
7
8
stage
actin
Vkg-GFP
Follicle cells migrate on the inner surface of the BM, which does not move
basal
apical
migration
The migrating follicle cells create fibril-like structures in the BM
Vkg-GFP
before migration
after migration
B
mouse RTVGGGQKV
zebrafish RTVGGGQKV
C.elegans IEQGGGQKI
Drosophila QKPGGGFKL
N26-5 QKPGDGFKL
Plod N26-5
(G75 to D)
1
722
glycosyl transferase
lysyl hydroxylase
C
Plod RNAi
Vkg
ER Tracker
D
Plod RNAi
Vkg
ER Tracker

Figure S1. Overview of BM remodeling, *Plod* mutant lesion and RNAi phenotype, Related to Figure 1

(A) Overview of BM remodeling during the early stages of egg chamber elongation. Actin is in red and Vkg-GFP is in green. The first image (ovariole) is a composite of three focal planes. Panel based on (Bilder and Haigo, 2012).

(B) The *Plod*$^{N26\text{-}5}$ lesion changes a highly conserved glycine at position 75 to aspartic acid.

(C) *Plod-RNAi causes* Vkg-GFP to accumulate in the basal cell cytoplasm. ER tracker shows that this organelle extends throughout the cytoplasm. Scale bar is 10 μm.

(D) Blowup of a single follicle cell showing the dark spot in the ER tracker signal where the ER membranes are distended and Col IV is trapped (arrow). Scale bar is 5 μm.

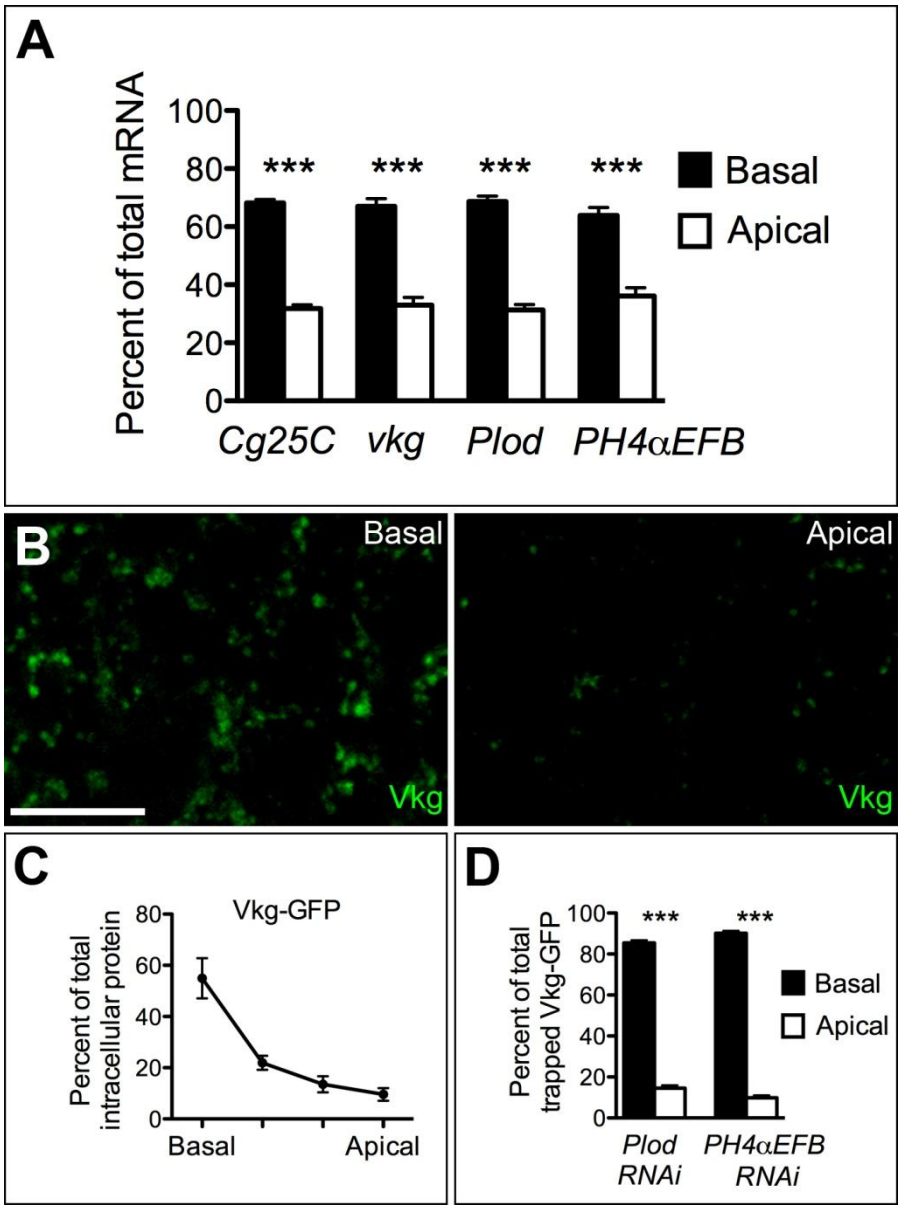

Figure S2. Quantification of the basal enrichment of Col IV protein and the Col IV-associated mRNAs, Related to Figure 2

(A) Quantification of mRNA levels in the basal half of the follicle cell cytoplasm vs. the apical half for *Cg25C*, *vkg*, *Plod* and *PH4αEFB* mRNAs. n=7-10 egg chambers for each condition.
(B) More Vkg-GFP fluorescence is observed in an optical section taken near the basal cell surface when compared to a section near the apical cell surface. Scale bar is 10 μm.
(C) Quantification of intracellular Vkg-GFP levels along the apical-basal axis in wild-type cells. n=7 groups of 8-10 cells each. Data represent mean ± SD.
(D) Quantification of trapped intracellular Vkg-GFP levels in the basal vs. apical cytoplasm in *Plod-RNAi* and *PH4αEFB-RNAi.* n=5 egg chambers for each condition.
(A and D) Data represent mean ± SEM, t-test: *** = P<0.0001.

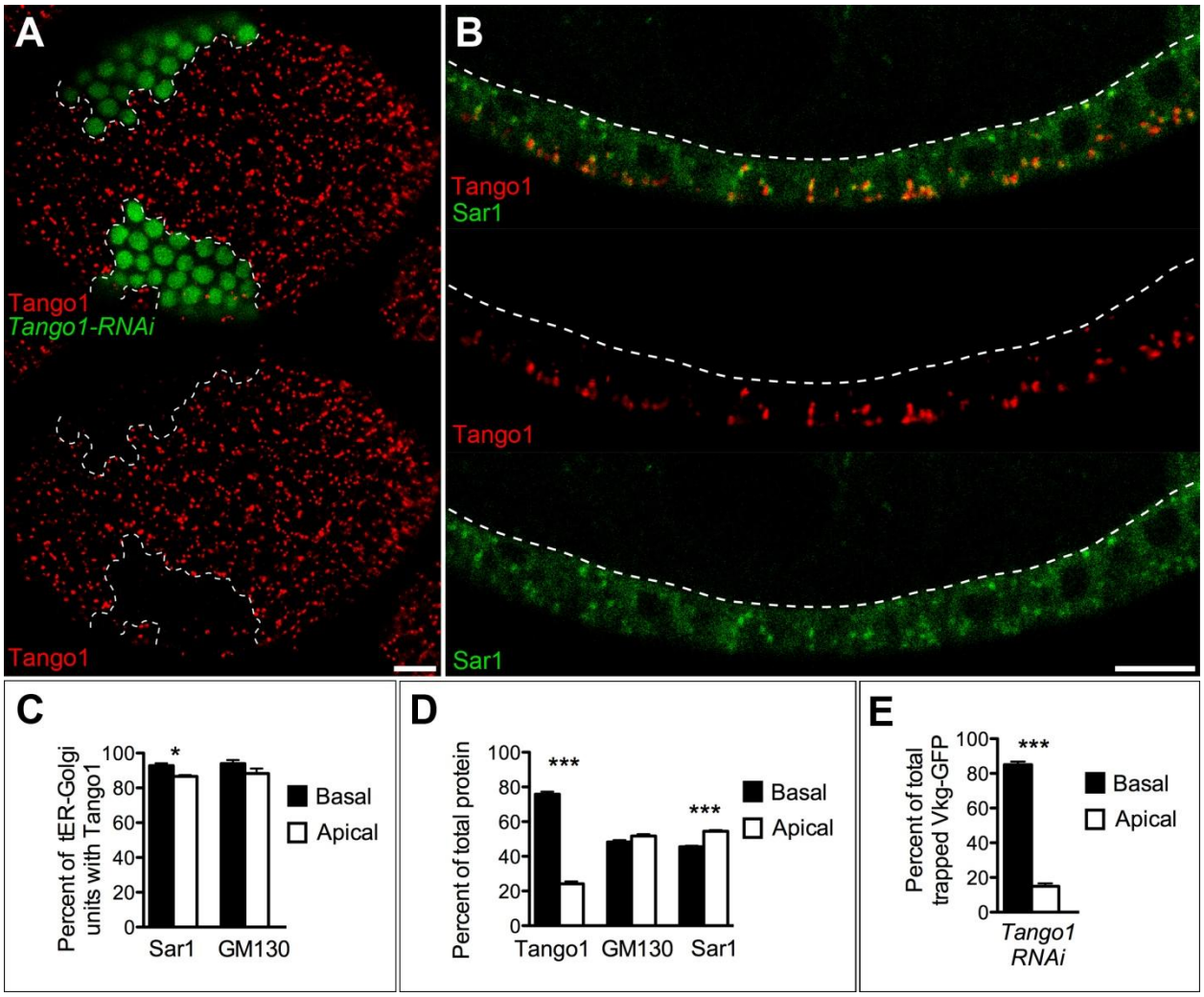

Figure S3. Tango 1 antibody validation and protein distribution, Related to Figure 3

(A) Follicle cell clones expressing *Tango1-RNAi* (GFP) effectively deplete the antibody signal, validating antibody specificity. Dashed lines mark clone boundaries. Scale bar is 10 μm.

(B) Although Sar1-GFP marks ER exit sites throughout the cell, the strongest Tango1 signal co-localizes with Sar1 at basal sites. Dashed lines mark the apical surface. Scale bar is 10 μm.

(C) Tango1 is present at the majority of tER-Golgi units, as visualized with Sar1 and GM130. n=200 punctae per protein in 4 egg chambers.

(D) Quantification of protein levels in the basal vs. apical cytoplasm shows that, while general tER-Golgi proteins like Sar1 and GM130 are fairly evenly distributed between these two domains, Tango1 is enriched basally. n=5 egg chambers.

(E) *Tango1-RNAi* causes Vkg-GFP to preferentially accumulate in the basal ER. n=5 egg chambers.

(C-E) Data represent mean ± SEM, t-test * = P<0.05, *** = P<0.0001.

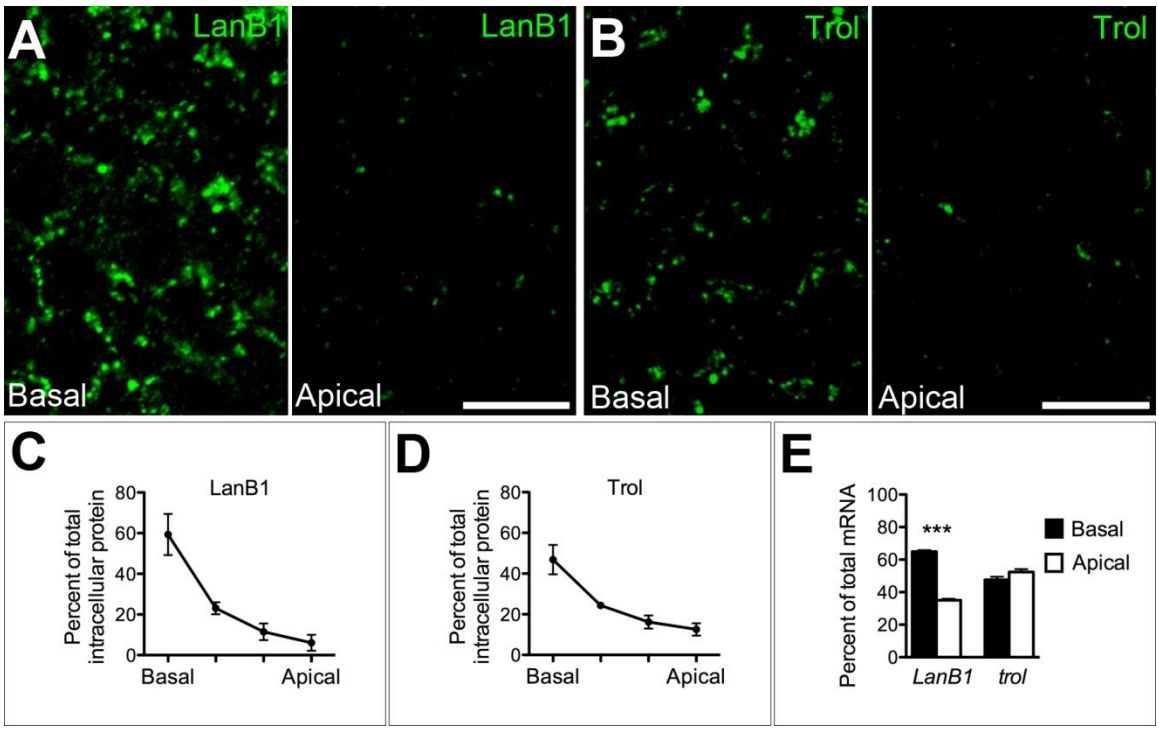

Figure S4. Quantification of intracellular protein and mRNA for Laminin and Trol, Related to Figure 4

(A and B) More (A) LanB1 and (B) Trol fluorescence is observed in an optical section taken near the basal cell surface compared to a section near the apical cell surface. Scale bars are 10 μm.
(C and D) Quantification of intracellular LanB1 and Trol levels along the apical-basal axis in wild-type cells. n=7-12 groups of 8-10 cells each. Data represent mean ± SD.
(E) Quantification of *LanB1* and *trol* mRNA levels in the basal vs. apical cytoplasm. n=6-7 egg chambers each. Data represent mean ± SEM, t-test *** = P<0.0001.

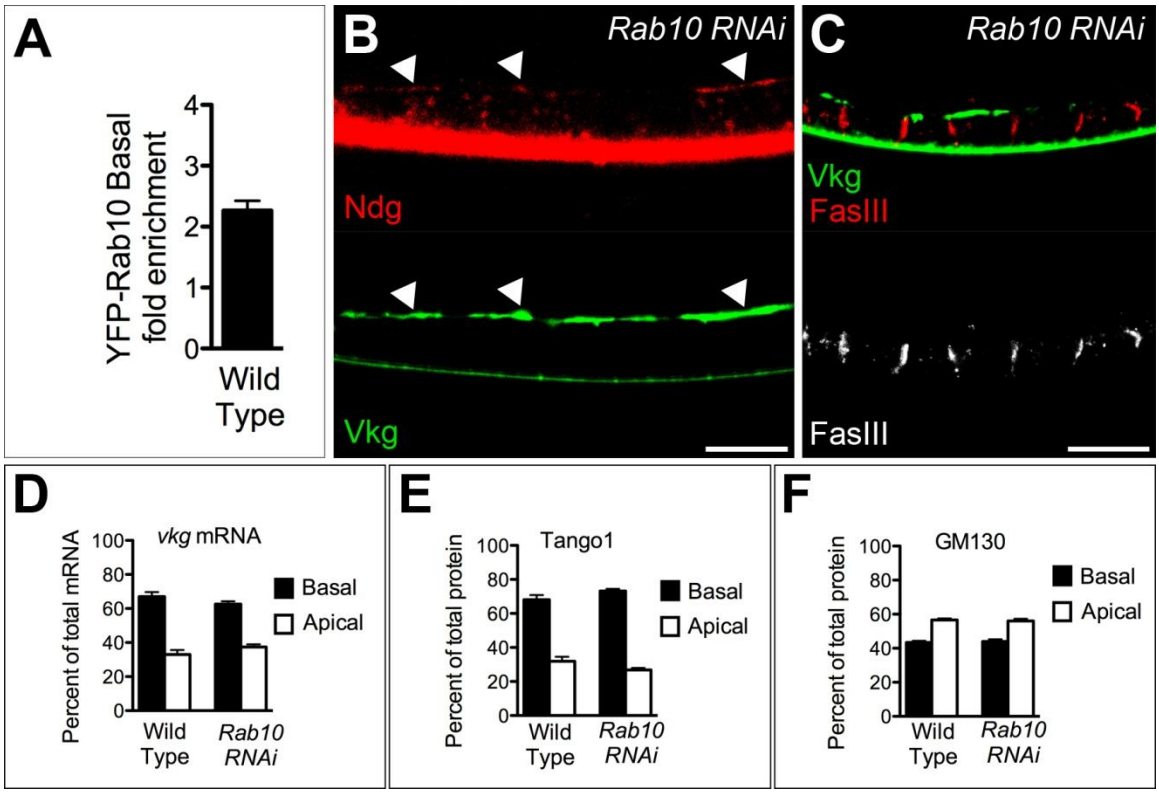

Figure S5. Rab10 promotes polarized BM secretion, Related to Figure 5
(A) Quantification of the fold enrichment of YFP-Rab10 at the basal surface vs. the apical surface. n=14 groups of 8-10 cells each. Data represent mean ± SEM.
(B) *Rab10-RNAi* causes weak accumulation of Nidogen on the apical surface (arrowheads).
(C) *Rab10-RNAi* has no effect on the localization of FasIII to the lateral cell membranes.
(B and C) The accumulation of Vkg-GFP on the apical surface confirms Rab10 knockdown. Scale bars are 10 μm.
(D-F) The apical-basal distributions of (D) *vkg* mRNA (E) Tango1 and (F) GM130 are unchanged under *Rab10-RNAi* conditions. n=6-14 egg chambers for each condition. Data represent mean ± SEM.

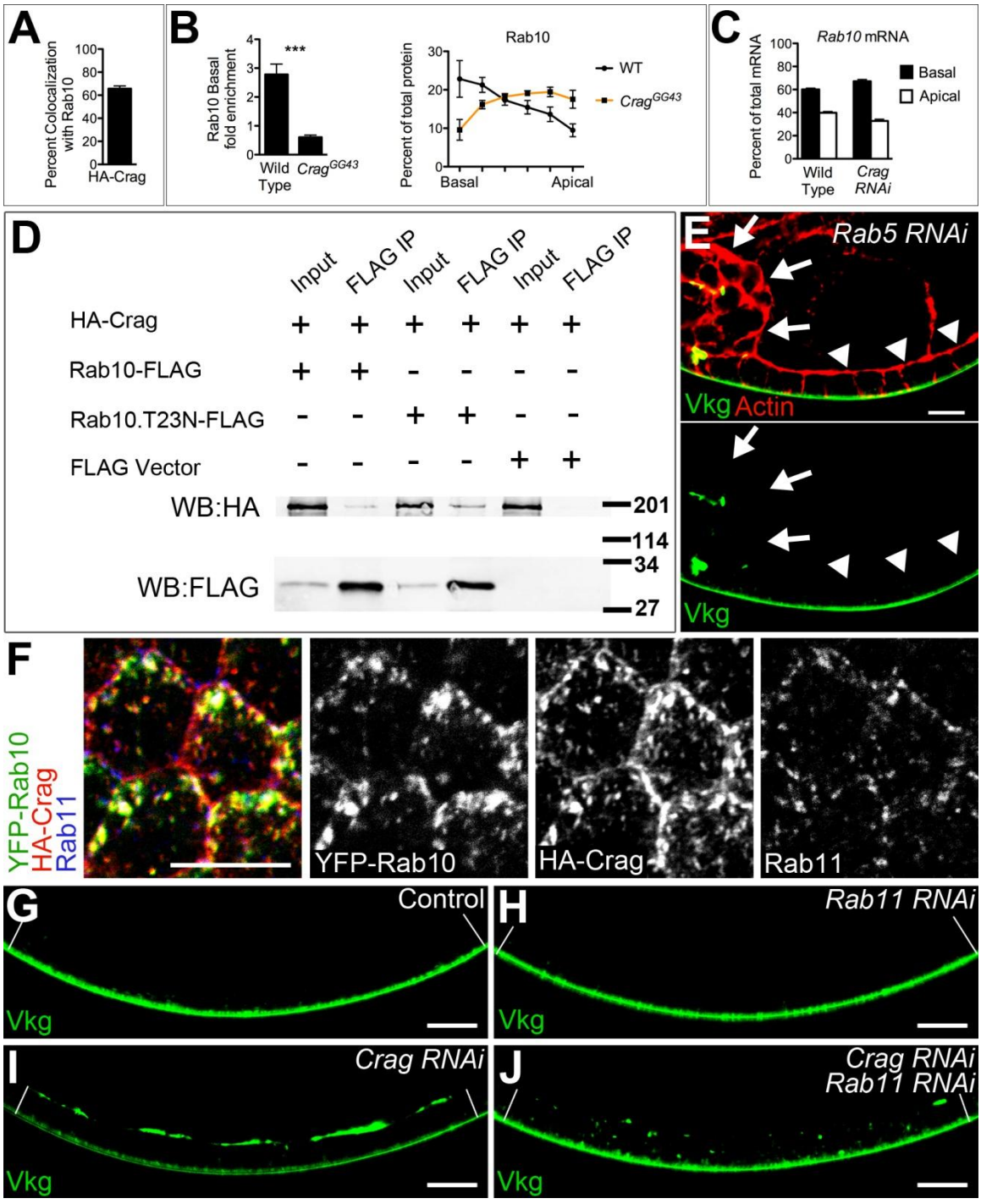
A
Percent Colocalization with Rab10
HA-Crag
B
Rab10 Basal fold enrichment
***
Wild Type
Crag^GG43
Rab10
Percent of total protein
WT
Crag^GG43
Basal
Apical
C
Rab10 mRNA
Percent of total mRNA
Basal
Apical
Wild Type
Crag RNAi
D
Input
FLAG IP
Input
FLAG IP
Input
FLAG IP
HA-Crag
Rab10-FLAG
Rab10.T23N-FLAG
FLAG Vector
WB:HA
WB:FLAG
201
114
34
27
E
Rab5 RNAi
Vkg Actin
Vkg
F
YFP-Rab10
HA-Crag
Rab11
YFP-Rab10
HA-Crag
Rab11
G
Control
Vkg
H
Rab11 RNAi
Vkg
I
Crag RNAi
Vkg
J
Crag RNAi
Rab11 RNAi
Vkg

Figure S6. Crag regulates Rab10 during polarized BM secretion, Related to Figure 6

(A) When an optical section is taken near the basal follicle cell surface, >60% of the Rab10 protein co-localizes with Crag. n=5 egg chambers.

(B) Quantification of the change in Rab10's apical-basal distribution in *Crag*^{GG43} mutant clones. n=7-9 groups of 8-10 cells each.

(C) *Rab10* mRNA shows some basal enrichment in wild-type cells, which remains under *Crag-RNAi* conditions. n=7-11 egg chambers.

(A-C) Excluding line graph in (B), data represent mean ± SEM, t-test *** = P<0.0001. Line graph data in (B) represent mean ± SD.

(D) HA-Crag consistently co-immunoprecipitated with Rab10-FLAG but not empty FLAG vector in 5 independent experiments. HA-Crag always demonstrated the strongest co-immunoprecipitation with Rab10.T23N-FLAG, consistent with Crag acting as a Rab10 GEF.

(E) *Rab5-RNAi* causes multi-layering of follicle cells at the egg chamber poles (arrows), as previously reported. However, the follicle cells that maintain their cuboidal morphology show no defects in polarized Vkg-GFP secretion (arrowheads).

(F) An optical section through the basal cytoplasm showing the co-localization of YFP-Rab10, HA-Crag, and Rab11.

(G and H) Vkg-GFP localization is normal in (G) wild-type and (H) Rab11-depleted follicle cells.

(I) Crag depletion causes Vkg-GFP to accumulate on the apical surface.

(J) Co-depletion of Crag and Rab11 eliminates the Vkg-GFP at the apical surface and increases the cytoplasmic signal.

(G-J) White lines extend between the apical and basal surfaces. Scale bars are 10 μm.

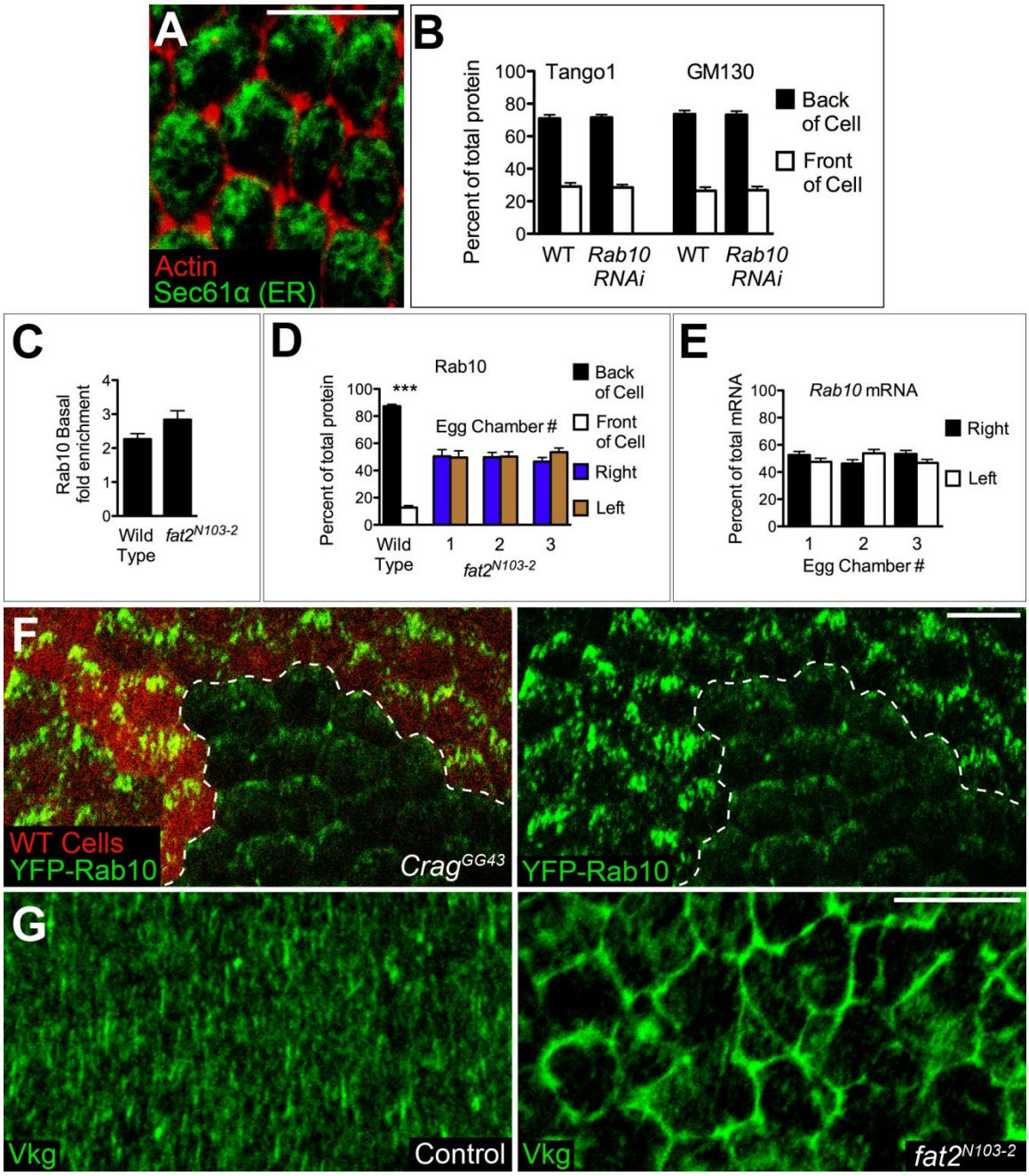
A
Actin
Sec61α (ER)
B
Percent of total protein
Tango1
GM130
Back of Cell
Front of Cell
WT
Rab10 RNAi
C
Rab10 Basal fold enrichment
Wild Type
fat2N103-2
D
Rab10
***
Egg Chamber #
E
Rab10 mRNA
Percent of total mRNA
Right
Left
F
WT Cells
YFP-Rab10
CragGG43
G
Vkg
Control
fat2N103-2

Figure S7. The BM exocytic machinery is planar polarized at the basal epithelial surface, Related to Figure 7

(A) Sec61α-GFP shows a planar polarized distribution near the basal follicle cell surface.

(B) Quantification of Tango1 and GM130 punctae in the basal cytoplasm reveals that the planar polarization of tER-Golgi units is unchanged under *Rab10-RNAi* conditions. n=6 egg chambers, 10 cells each.

(C) Rab10's basal enrichment is unchanged in $fat2^{N103\text{-}2}$ epithelia. n=14-15 groups of 8-10 cells each.

(D) Rab10's planar polarization is lost in $fat2^{N103\text{-}2}$ epithelia. For $fat2^{N103\text{-}2}$ epithelia, measurements from three individual egg chambers are shown, because it is not possible to distinguish the front and back of each cell (see methods). n=3 egg chambers, 10 cells each.

(E) *Rab10* mRNA is not polarized along the planar epithelial axis. n=33 cells from each of the 3 egg chambers shown in the graph. Again, it is not possible to determine each cell's front from back under these conditions.

(B-E) Data represent mean ± SEM, t-test *** = P<0.0001.

(F) Although Rab10's basal enrichment is largely abrogated in $Crag^{GG43}$ mutant cells, the Rab10 protein that is still present basally is polarized normally along the planar axis. The dashed line marks the clone boundary.

(G) $fat2^{N103\text{-}2}$ epithelia show severe defects in BM structure compared to wild-type epithelia. Scale bars are 10 μm.

Supplemental Experimental Procedures

Detailed experimental genotypes

figure	panels	genotype
1	B	*w; e22c-Gal4, UAS-FLP/ +; ubi-eGFP FRT80/ +*
	C	*w; e22c-Gal4, UAS-FLP/ +; Plod$^{N26\text{-}5}$, FRT80/ ubi-eGFP FRT80*
	D	*w; tj-Gal4/ UAS-Plod-RNAi^{v45486}*
	E	*w; e22c-Gal4, UAS-FLP/ vkg-GFP; FRT80/ ubi-eGFP, FRT80*
	F	*w; e22c-Gal4, UAS-FLP/ vkg-GFP; Plod$^{N26\text{-}5}$, FRT80/ ubi-eGFP, FRT80*
	G	*w; tj-Gal4/ UAS-Plod-RNAi^{v45484}*
2	A B C D	*w^{1118}*
	E	*tj-Gal4, vkg-GFP/ +; UAS-PH4αEFB-RNAi$^{TRiP.HMS00835}$/ +*
3	A	*w^{1118}*
	B	*w, vkg-GFP*
	C	*tj-Gal4, vkg-GFP/ +; UAS-Tango1-RNAi^{v21594}/ +*
4	A B	*tj-Gal4, vkg-GFP/ +; UAS-Tango1-RNAi^{v21594}/ +* *tj-Gal4, vkg-GFP/ +*
	C	*w^{1118}*
	D	*w, trol-GFP*
5	A	*tj-Gal4/ P{UASp-YFP.Rab10}13*
	B	*tj-Gal4, vkg-GFP/ +; UAS-Rab10-RNAi$^{TRiP.JF02058}$/ +*
	C	*trol-GFP/ +; tj-Gal4/ +; UAS-Rab10-RNAi$^{TRiP.JF02058}$/ +*
	D	*vkg-GFP; TubP-Gal4/ UAS-Rab10-RNAi$^{TRiP.JF02058}$*
	E F G	*vkg-GFP/+; TubP-Gal4/ UAS-Rab10-RNA$^{TRiP.iJF02058}$*
6	A	*TubP-Gal80^{ts}/ P{UASp-YFP.Rab10}13; TubP-Gal4 /UASp-HA-CragA (53A)*
	B	*Crag^{GG43}, FRT19A/ ubi-mRFP, w, hs-FLP, FRT19A; tj-Gal4/ P{UASp-YFP.Rab10}13*
	C G	*tj-Gal4, vkg-GFP/ +*
	D	*tj-Gal4, vkg-GFP/+; UASp-HA-CragA (53A)/ +*
	E	*tj-Gal4, vkg-GFP/ P{UASp-YFP.Rab10.T23N}15*
	F	*tj-Gal4, vkg-GFP/ P{UASp-YFP.Rab10.T23N}15; UASp-HA-CragA (53A)/ +*
	H	*tj-Gal4, vkg-GFP/ UAS-Rab11-RNAi*
	I	*tj-Gal4, vkg-GFP/ +; UAS-Rab10-RNAi$^{TRiP.JF02058}$/ +*
	J	*tj-Gal4, vkg-GFP/ UAS-Rab11-RNAi; UAS-Rab10-RNAi$^{TRiP.JF02058}$/ +*
7	A	*tj-Gal4, vkg-GFP/ P{UASp-YFP.Rab10.T23N}15*
	B D E G	*tj-Gal4/ P{UASp-YFP.Rab10}13*
	C F	*tj-Gal4/ P{UASp-YFP.Rab10}13; fat2$^{N103\text{-}2}$, FRT80*
S1	C D	*w; tj-Gal4, vkg-GFP / UAS-Plod-RNAi^{v45486}*
S2	A	*w^{1118}*

	B C	*w, vkg-GFP*
	D	*tj-Gal4, vkg-GFP/ +; UAS-PH4αEFB-RNAi$^{TRiP.HMS00835}$/ +* *w; tj-Gal4, vkg-GFP / UAS-Plod-RNAi^{v45486}*
S3	A	*hs-Flp;; Act5c>>Gal4, UAS-eGFP/ UAS-Tango1-RNAi^{v21594}*
	B C D	*Sar1-GFP/ +*
	E	*tj-Gal4, vkg-GFP/ +; UAS-Tango1-RNAi^{v21594}/ +*
S4	A B C D	*w, vkg-GFP (stained with LanB1 and Trol antibodies)*
	E	*w^{1118}* *w, trol-GFP*
S5	A	*tj-Gal4/ P{UASp-YFP.Rab10}13*
	B C	*vkg-GFP/+; TubP-Gal4/ UAS-Rab10-RNA$^{TRiP.iJF02058}$*
	D	*w^{1118}* *vkg-GFP/ +; TubP-Gal4/ UAS-Rab10-RNAi$^{TRiP.JF02058}$*
	E F	*vkg-GFP/ +; TubP-Gal4/ +* *vkg-GFP/ +; TubP-Gal4/ UAS-Rab10-RNAi$^{TRiP.JF02058}$*
S6	A	*tj-Gal4/ P{UASp-YFP.Rab10}13; UASp-HA-CragA (53A)/ +*
	B	*Crag^{GG43}, FRT19A/ ubi-mRFP, w, hs-FLP, FRT19A; tj-Gal4/ P{UASp-YFP.Rab10}13*
	C	*w^{1118}* *tj-Gal4, vkg-GFP/ +; UAS-Crag-RNAi$^{TRiP.HMS00241}$/ +*
	E	*UAS-Rab5-RNAi^{v34094}/ +; tj-Gal4, vkg-GFP/ +*
	F	*TubP-Gal80^{ts}/ P{UASp-YFP.Rab10}c13; TubP-Gal4 /UASp-HA-CragA (53A)*
	G	*tj-Gal4, vkg-GFP/ +*
	H	*tj-Gal4, vkg-GFP/ UAS-Rab11-RNAi*
	I	*tj-Gal4, Vkg-GFP/ +; UAS-Crag-RNAi$^{TRiP.HMS00241}$/ +*
	J	*tj-Gal4, Vkg-GFP/ UAS-Rab11-RNAi; UAS-Crag-RNAi$^{TRiP.HMS00241}$/ +*
S7	A	*Sec61α-GFP/ SM6a*
	B	*vkg-GFP/ +; TubP-Gal4/ +* *vkg-GFP/ +; TubP-Gal4/ UAS-Rab10-RNAi$^{TRiP.JF02058}$*
	C	*tj-Gal4/ P{UASp-YFP.Rab10}13* *tj-Gal4/ P{UASp-YFP.Rab10}13; fat2^{N103-2}, FRT80*
	D	*tj-Gal4/ P{UASp-YFP.Rab10}13; FRT80* *tj-Gal4/ P{UASp-YFP.Rab10}13; fat2^{N103-2}, FRT80*
	E	*w^{1118}*
	F	*Crag^{GG43}, FRT19A/ ubi-mRFP, w, hs-FLP, FRT19A; tj-Gal4/ P{UASp-YFP.Rab10}13*
	G	*vkg-GFP; FRT80* *vkg-GFP; fat2^{N103-2}, FRT80*
Movie	S1	*tj-Gal4/ P{UASp-YFP.Rab10}13*
Movie	S2	*tj-Gal4/ P{UASp-YFP.Rab10}13; fat2^{N103-2}, FRT80*
Movie	S3	*tj-Gal4/ P{UASp-YFP.Rab10}13*

Conditions for transgene expression

Most crosses were raised, and experiments performed at 25°C. Experiments using different conditions are detailed below.

figure	panels	temp at which cross was raised	females on yeast	
			temp	no. days
3	C	RT	25 °C	1
4	A B	RT	RT	2
5	B-G	25 °C	29 °C	3
6	A	18 °C	25 °C	2
6	C-F	RT	29 °C	4
6	G-J	18 °C	25 °C	1.5
S6	E	RT	RT	3
S6	G-J	18 °C	25 °C	1.5

Identification of the *Plod*$^{N26\text{-}5}$ lesion

We found that the *N26-5* round egg mutation failed to complement *Df(3L)ED4470*. This deficiency removes the 68A6-68E1 chromosomal region, containing the *Plod* gene. *N26-5, FRT80* was placed over the *TM3, twi-GFP* balancer, and DNA was extracted from GFP-negative first instar larvae. PCR products covering the Plod coding regions were ExoSap-treated, directly sequenced and compared to analogous products from *FRT80* controls.

Electron microscopy

Ovaries were removed in 2% glutaraldehyde in 0.1M Na cacodylate buffered at pH 7.4 at 25°C for 10 minutes and then placed on ice for 30 to 50 minutes. They were rinsed in cold buffer, and then post-fixed in 2% OsO_4 in 0.1M Na cadodylate for 2 hr at 4°C. After a cold water wash, they were stained in 1% uranyl acetate overnight at 4°C. Ovaries were dehydrated in ethanol, and then embedded in epoxy resin (DER732/332 mixture). 70 to 80 nm thin sections were stained

with uranyl acetate and lead citrate and viewed in a Technai F30 electron microscope at 300kV. Photographs were taken with a Gatan digital camera.

In situ hybridization probe primers

Blue text indicates the position of the T7 promoter sequence

gene	primers used for probe production	
vkg	F	GTCTCTCTGGTGATGATGGACCGGA
	R	TAATACGACTCACTATAGGGTCTCCCTGCTCACCAATCAATCCGC
Cg25C	F	GTCGCCAAGGTAACTTTGGACCCCA
	R	TAATACGACTCACTATAGGGGCCAGGTATGCCAGCATCTCCCTTAG
LanB1	F	GCAGATGAATCCCAGGGTAAAGCCAAG
	R	TAATACGACTCACTATAGGGCCAATCTACGTATAGCACTGCCTGTAGTG
Plod	F	GGTATCTTCATGTACGCCAGCAATC
	R	TAATACGACTCACTATAGGGAAGGCGCGCTCCTGCAGC
PH4αEFB	F	CCCGTGGCCAAGAGTGACCC
	R	TAATACGACTCACTATAGGGCCTGGCAAAATCAAAGTGCGGCTCG
Rab10	F	CAAAACTCCGAACGATGGAT
	R	TAATACGACTCACTATAGGGCAGAGCAGGGCGTACATCAC

Tango1 antibody production

A PCR product corresponding to amino acids 272-653 of Tango1 was cloned into the pGEX-Ext vector (Hakes and Dixon, 1992). The GST-fusion protein was expressed in *E. coli*, purified using Glutathione-Sepharose (GE Healthcare), and injected into guinea pigs (Pocono Rabbit Farm and Laboratory Inc.). Antibodies were purified from serum using saturated Ammonium sulfate.

Production of Rab10-FLAG and Rab10.T23N-FLAG Expression Constructs

The Rab10 coding sequence was PCR-amplified from genomic DNA isolated from UAS-YFP-Rab10 flies (BL 9789). The PCR product was gel extracted, digested with BamHI and XhoI and cloned into the Gateway pENTR3C Dual Selection Entry Vector (Invitrogen). QuikChange II XL

Site-Directed Mutagenesis (Agilent) was used to create the Rab10.T23N mutation. Both the Rab10 and Rab10.T23N inserts were recombined (LR clonase reaction) into the pAWF Gateway expression vector (actin promoter, 3X C-terminal FLAG tag - Invitrogen).

Crag and Rab10 physical interaction

The physical interaction between Crag and Rab10 was confirmed using *UAS-HA-Crag* (Denef et al., 2008), and the Rab10-FLAG and Rab10.T23N-FLAG constructs described above. 8.0×10^6 S2 cells were transfected using DDAB (dimethyldioctadecyl-ammonium bromide) at 250 µg/ml (Sigma-Aldrich). *Ubiquitin-Gal4* was co-transfected with *UAS-HA-Crag* to drive expression. IPs were performed 2 days after transfection. Cells were harvested and lysed in buffer containing 50 mM Hepes, 150 mM NaCl, 1 mM EDTA, 0.5 mM EGTA, 0.9 M glycerol, 0.1% Triton X-100, 0.5 mM DTT, and complete protease inhibitor cocktail (Roche). Flag IP reactions were performed using anti-Flag M2 agarose beads (Sigma-Aldrich) at 4°C for 2 h. 2% of the total lysate and 50% of the immunoprecipitate from transfected S2 cells were analyzed via Western Blot using the following antibodies: mouse anti-FLAG M2 at 1:20,000 (Sigma- Aldrich) and rabbit anti-HA at 1:5,000 (Rockland). The following secondary antibodies were used at 1:5000: goat anti-rabbit Irdye700 (LI-COR Biosciences) and goat anti-mouse Irdye800 (Rockland). Blots were imaged using Odyssey software version 2.1 (LI-COR Biosciences).

Quantification of mRNA and protein levels in the basal vs. apical cytoplasm.

This method was used to determine the relative fluorescence levels in the basal vs. apical cytoplasm for mRNAs, ER-trapped BM proteins, Tango1, Sar1 and GM130. Analyses were performed on transverse optical sections of stage 7-8 egg chambers. Using imageJ, the follicle cell epithelium was isolated from the germ cell cluster and separated into apical and basal halves. For BM proteins, the basal-most portion of the epithelium was also removed to avoid the inclusion of extracellular signal. Mean fluorescent signal intensity was measured in each

epithelial half and normalized to total mean fluorescence. Graphing and statistical analyses were performed using Prism software (GraphPad).

Quantification of the basal enrichment of intracellular BM proteins in wild-type cells

Because of the intense, extracellular signal from the BM, it was not possible to accurately quantify intracellular BM protein levels in transverse optical sections. Therefore, a four-slice Z-stack was taken between the apical epithelial surface and the basal-most plane that did not include the BM on stage 7-8 egg chambers. The mean fluorescent intensity was measured for each slice and normalized as the percentage of the combined intensity of all slices. Averages with standard deviations are plotted for each Z plane. Graphing and statistical analyses were performed using Prism software (GraphPad).

Quantification of the basal enrichment of YFP-Rab10

In addition to general cytoplasmic staining, there is a strong YFP-Rab10 signal tightly associated with the basal follicle cell surface. To quantify this basal enrichment, we generally compared the fluorescence intensity of YFP-Rab10 in optical sections taken at the basal vs. apical surfaces to determine the "basal fold enrichment" of this signal. However, a second method was used to better represent the change in Rab10's distribution in *Crag* cells. Six-slice Z-stacks were taken between the basal and apical surfaces of *Crag* mosaic epithelia. The mean fluorescence intensity was then measured for equivalent regions of mutant and wild-type cells for each slice, and was normalized as a percentage of the combined intensity of all slices. Averages with standard deviations were plotted for each slice. All data is from stage 7-8 egg chambers. Graphing and statistical analyses were performed using Prism software (GraphPad).

Quantification of the co-localization of Tango1 with Sar1 and GM130

This method was used to determine whether Tango1 is present at all tER-Golgi sites. Analyses were performed on transverse optical sections of stage 7-8 egg chambers. Using imageJ, 15-20 follicle cells were isolated from the germ cell cluster and separated into apical and basal halves. All Sar1 punctae were circled manually, and then the percentage of circles that also contained Tango1 signal was determined. This process was repeated with the cis-Golgi marker GM130, as it gives a cleaner signal. Graphing and statistical analyses were performed using Prism software (GraphPad).

Quantification of the co-localization between Rab10 and Crag

Optical sections near the basal epithelial surface were processed in ImageJ using the threshold function on the automatic setting. A custom MATLAB script (*available upon request*) was then used to determine the percentage of co-localized pixels between the Rab10 and Crag signals. All data is from stage 7-8 egg chambers. Graphing and statistical analyses were performed using Prism software (GraphPad).

Quantification of the planar polarization of mRNAs and proteins in the basal cytoplasm

Starting from an optical section taken near the basal epithelial surface, each cell was split into front and back halves based on the position of the egg chamber's AP axis and of forward-facing actin-based protrusions. Protein and mRNA levels were quantified either by counting punctae (Tango1 and GM130) or measuring mean fluorescence intensity (YFP-Rab10 and *Rab10* mRNA) in each half. In *fat2*^{N1032} epithelia and those stained for mRNA, it was not possible to use protrusions to mark the cell's leading edge. In these cases, each cell was split in half along the egg chamber's AP axis and the halves were called "right" or "left" based on their orientation when viewed from the egg chamber's anterior pole. In wild type, forward-facing protrusions can

be on either the right or left in a given egg chamber. All data is from stage 7-8 egg chambers.

Graphing and statistical analyses were performed using Prism software (GraphPad).

Supplemental References

Bilder, D., and Haigo, S.L. (2012). Expanding the morphogenetic repertoire: perspectives from the Drosophila egg. Dev Cell *22*, 12-23.

Denef, N., Chen, Y., Weeks, S.D., Barcelo, G., and Schupbach, T. (2008). Crag regulates epithelial architecture and polarized deposition of basement membrane proteins in Drosophila. Dev Cell *14*, 354-364.

Hakes, D.J., and Dixon, J.E. (1992). New vectors for high level expression of recombinant proteins in bacteria. Anal Biochem *202*, 293-298.